Mixing enhancement in microchannel by changing parameters of thermal waves using TVEC effect

Author

Muhammad Asif

Reg. Number

00000274497

Supervisor

Dr. Niaz Bahadur Khan

DEPARTMENT OF MECHANICAL ENGINEERING

SCHOOL OF MECHANICAL & MANUFACTURING ENGINEERING

NATIONAL UNIVERSITY OF SCIENCES AND TECHNOLOGY

ISLAMABAD

July 2021

Mixing enhancement in microchannel by changing parameters of thermal waves using TVEC effect

Author

Muhammad Asif

Reg. No.

00000274497

A thesis submitted in partial fulfillment of the requirements for the degree of

MS Mechanical Engineering

Thesis Supervisor:

Dr. Niaz Bahadur Khan

Thesis Supervisor's Signature: _____

DEPARTMENT OF MECHANICAL ENGINEERING

SCHOOL OF MECHANICAL & MANUFACTURING ENGINEERING

NATIONAL UNIVERSITY OF SCIENCES AND TECHNOLOGY,

ISLAMABAD

July 2021

Thesis Acceptance Certificate

It is certified that the final copy of MS Thesis written by **Muhammad Asif** (Registration No. **00000274497**), of Department of **School of Mechanical and Manufacturing Engineering (SMME)** has been vetted by undersigned, found complete in all respects as per NUST statutes / regulations, is free from plagiarism, errors and mistakes are accepted as a partial fulfillment for award of MS Degree. It is further certified that necessary amendments as pointed out by GEC members of the scholar have also been incorporated in this dissertation.

Signature: _____

Date: _____

Dr. Niaz Bahadur Khan (Supervisor)

Signature HOD: _____

Date: _____

Signature Principal: _____

Date: _____

Declaration

I certify that this research work titled "Mixing enhancement in microchannel by changing parameter of thermal waves using TVEC effect" is my own work. The work has not been presented elsewhere for assessment. The material that has been used from other sources it has been properly acknowledged / referred.

Signature of Student
Muhammad Asif
Reg. No.
00000274497

Plagiarism Certificate (Turnitin Report)

This thesis has been checked for Plagiarism. Turnitin report endorsed by Supervisor is attached.

Signature of Student

Muhammad Asif

Registration Number

00000274497

Signature of Supervisor

Dr. Niaz Bahadur Khan

Copyright Statement

- Copyright in text of this thesis rests with the student author. Copies (by any process) either in full, or of extracts, may be made only in accordance with instructions given by the author and lodged in the Library of NUST School of Mechanical & Manufacturing Engineering (SMME). Details may be obtained by the Librarian. This page must form part of any such copies made. Further copies (by any process) may not be made without the permission (in writing) of the author.
- The ownership of any intellectual property rights which may be described in this thesis is vested in NUST School of Mechanical & Manufacturing Engineering, subject to any prior agreement to the contrary, and may not be made available for use by third parties without the written permission of the SMME, which will prescribe the terms and conditions of any such agreement.
- Further information on the conditions under which disclosures and exploitation may take place is available from the Library of NUST School of Mechanical & Manufacturing Engineering, Islamabad.

Acknowledgements

I am thankful to my Creator Allah Subhana-Watala to have guided me throughout this work at every step and for every new thought which You setup in my mind to improve it. Indeed, I could have done nothing without Your priceless help and guidance. Whosoever helped me throughout the course of my thesis, whether my parents or any other individual was Your will, so indeed none be worthy of praise but You.

I am profusely thankful to my beloved parents who raised me when I was not capable of walking and continued to support me throughout in every department of my life.

I would also like to express special thanks to my supervisor Dr. Niaz Bahadur Khan for his help throughout my thesis and for Continuum Mechanics course which he has taught me.

I would also like to pay special thanks to Mr. Muhammad Omair Khan for his tremendous support and cooperation. Each time I got stuck in something, he came up with the solution. Without his help I would not have been able to complete my thesis. I appreciate his patience and guidance throughout the whole thesis.

I would also like to thank Dr. Emad Uddin, Dr. Zaib Ali and Dr. Muhammad Sajid for being on my thesis guidance and evaluation committee and express my special thanks to Dr. Niaz Bahadur Khan for his help. I am also thankful to Dr. Emad Uddin for their support and cooperation.

Finally, I would like to express my gratitude to all the individuals who have rendered valuable assistance to my study.

Dedicated to my exceptional parents and adored siblings whose tremendous support and cooperation led me to this wonderful accomplishment.

Abstract

Some basic level familiarity of micro fluidic mixers on their mixing comportment is mandated for the significance of micro reaction in micro mixers. The intention of the research is mainly development and usage of thermo viscous contraction and expansion consequence for the purpose of improving mixing ability in the micro mixers. Properly constant shape of flow in intellect of an average of time may be produced in the channels of the micro mixers by this effect of changing viscosity and density by wandering thermal waves at the opposite walls of channels. For achieving this goal 2D micro channel is well-thought-out in which statistical simulations of anarchy movement of fluid caused by episodic thermal limit state are done with different boundary conditions parameters. In unruly mixing of the fluids the influence of the Strouhal number, Reynold number and the heat dispersion extent estimation are the major aims of the paper. The extent of disorder is assessed by using the vorticity as norms for mixing improvement. It is concluded that the key of the anarchy micro mixing in the micro channels can be well-thought-out this thermal expansion and contraction consequence as a possible mean.

We investigate that engulfment as a primary parameter which is necessary to occur with the varying strain rate and vorticity creation in order to enhance mixing. Differential pressure effect on mixing increment is investigated thoroughly which is another source paying role to move the whole domain in micro channel while the thermo viscous expansion and contraction effect causes to mixing improving in micro channel. Final results reveal that the vorticity is predominantly a function of thickness of film and velocity of fluid which are dimensionless, and this whirling motion is created by variation of the viscosity and density of the fluid which is actually because of the difference in temperature at the boundary conditions where heat is transferred from boundary to the fluid flow.

Key Words: *Differential Pressure, thermos-viscous expansion and contraction effect (TVEC), Vorticity, Chaotic Mixing*

Table of Contents

List of Figures

List of Tables

CHAPTER 1: INTRODUCTION AND LITERATUTE REVIEW

In applications involving microfluidic motion, mixing is one of the simplest and difficult to achieve criteria. Many mixer designs have been developed for various fields of application, such as biological, nanoscale and environmental technology. However, users or designers of microfluidic mixers should be careful when choosing a mixer for their specific application, because papers or patents describing a design tend to emphasize advantages and seldom confirm disadvantages.

In the past five years, since two good review papers on microfluidic mixing were published in 2005 [1,2], number of papers have been circulated on the topic. We found that about 50 of these papers suggested new or improved designs and we demonstrated that their hybrid performance was identical or healthier than the conservative designs. In this analysis article, we summarized the ideological framework behind the proposed designs and discussed the pros and cons of each design in real-world applications.

Since most microfluidic applications involve liquids, we are limited to mixing liquids. Miscible liquids are clearly the source of our concern because we see diffusion as the final stage of the entire mixing process. Reynold number is 1 usually in microfluidic application. Therefore, papers proposing to design the mixers, which show superior performance mainly with advanced Reynolds numbers (for example, 10 or 100) are excluded in this review.

Jayawraj et al. [3] A review was offered for the investigation and experimentations of fluid flow and micro-channel mixing, but their review was mainly on the fiction issued before 2005. More recently, Falk and Komingi [4] proposed methods of performance evaluation or analysis. Micro-Mixer for Villermaux / Dushman Reaction Evaluation. They joint the order of volume analysis and phenotypes to originate the relationship amid mixing time and other constraints (such as the Reynolds number). Aubin et al. [5] Suggested experimental techniques for measuring the flow pattern, velocity, and mixing performance of fine blending. However, review papers were not found to evaluate the main topographies of different categories of micro mixers in relations of mixing routine, variety of applications, and manufacturing effort. This analysis paper recapitulates the basic ideas behind the proposed blender design. In published literature after 2005 and onwards, the range of application and difficulty of manufacturing.

1.1 Principles and Terminology of Fluid Mixing

There are many words that can be exploited for the description of microfluidic mixers with the same trouble without causing annoyance or anxiety. Contains vibration, arousal, arousal, bow, etc. Our purpose is not to differentiate between parts, but it is not our purpose, but we must emphasize it.

Reference [6] refers to the variance between mixing and moving, because the difference refers to the genuine procedure that takes place during the coupling. This means that the term "coupling" refers to a physical process that involves simultaneous conversion and conversion. The term blending here denotes most of the materialism, which must be joined together. In other arguments, we can roughly say that the direct mixing of the less conductive material occurs in two phases: the coupling in the first phase and the distribution in the second phase.

Presume we have two types of liquids in common, and our main passion is to mix drinks. See the picture 1. Even though the random motion of liquid particles can be seen everywhere, it does not appear to change significantly in the volume of each liquid away from the incoming connector, since all particles of each liquid have the same characteristics. Compared to the visual interface, the particles on mutually sections have distinct properties, so arbitrary cellular gesture will cause the particles to move in and out. This apparent phenomenon is called diffusion. Primarily, the border is very fast due to lack of interface, but continuous distribution will gradually split the two micros to the interface. This may have been the result of an arbitrary distribution process. The movement of an object through the interface is equivalent to the gradual evolution of something, called the law of volition, and the same contradictory definition is defined as the separation of the fruit. Figure 2 shows a specific micro-channel in which no mixed elements or structures have been identified. Two different liquids flow from different containers equivalent to each other, so there is no stirring, and the mixing is complete. We entitle C as the element (or concentration) of the fluid occupied by any small area through the fluids present A and B and then at the inlet of the channel (for example, in Fig.2 P0) where two liquids start. For continuation, area c = 0 in the upper half, lower half and c = 1. As shown in Fig. 2, the absorption circulation gradient gradually increases in the direction of P0 flow. However, the peak concentration up to point P1 does not change between c = 1 and c = 0. Moreover, the supreme and minutest values of c increase and decrease, correspondingly, and finally return to the final value of c = 0.5.

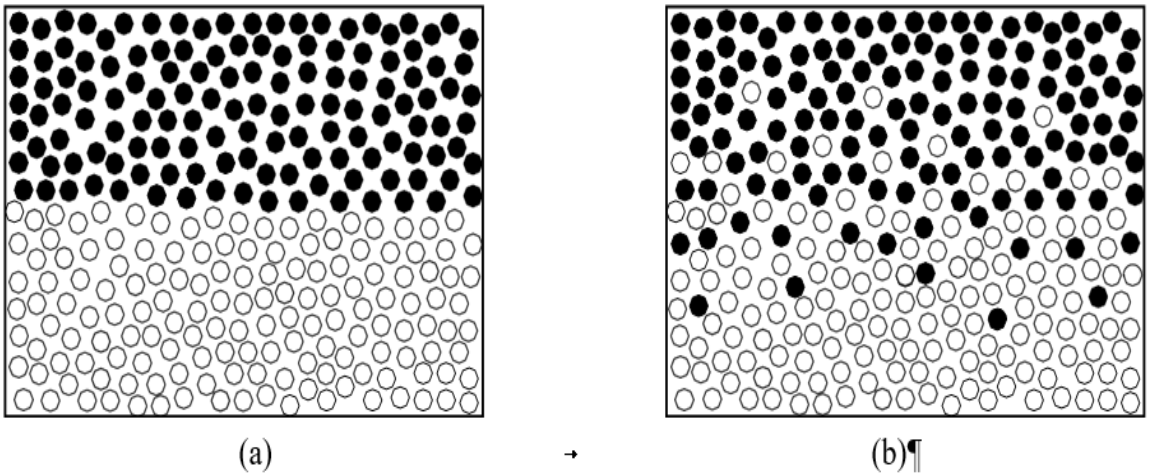

Figure 1: Illustration of Fluid mixing in (a) Initial (b) mixing stage.

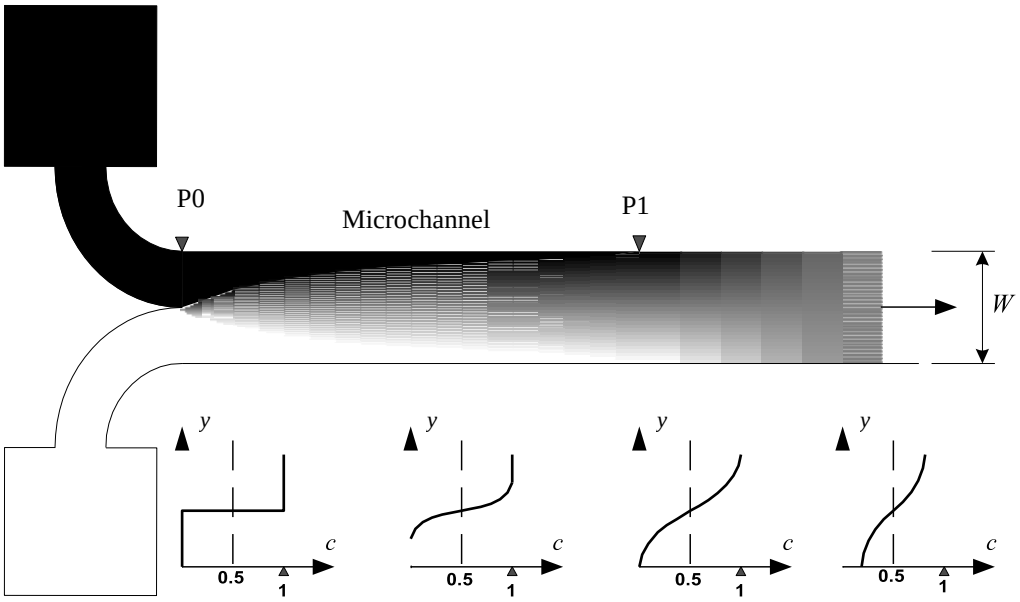

Figure 2: Concentration distribution in a channel

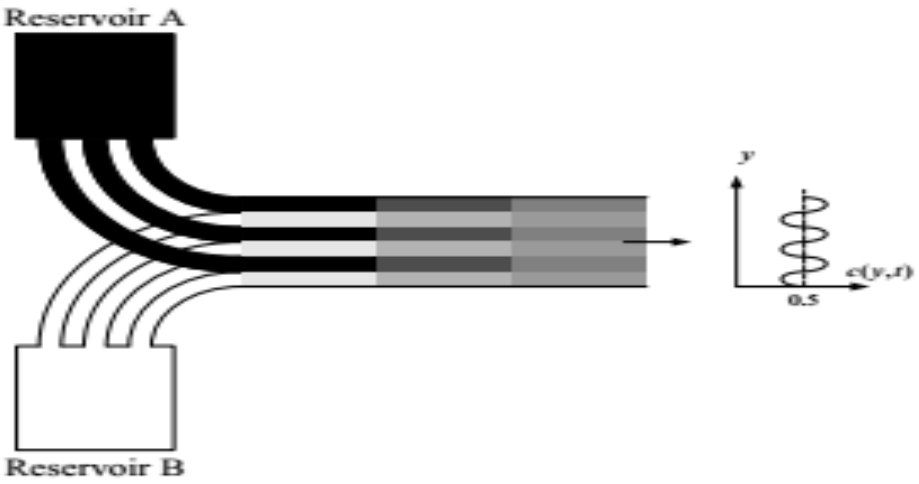

Figure 3: Illustration of Hydrodynamic micro channel focus

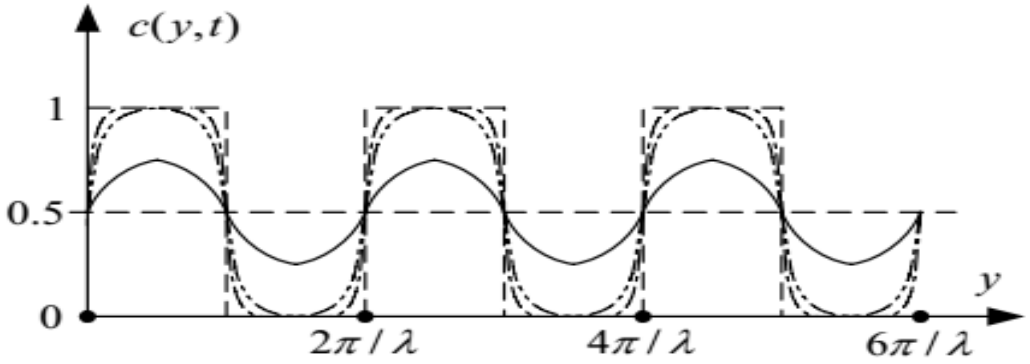

Figure 4: Schematic representation of development of concentration along the micro channel length

It is generally believed that the hilarity mixing structure is the best way of synthesis on a microscopic scale. Figure 5 shows the specific evolution of the stripe pattern and the focus distribution, obtained by the chaotic mixture obtained from the extreme model. In this move, we identified two dissimilar mechanisms that happen at the same time. The first is the expansion and coating of the liquid spray, which greatly reduces the thickness of the tape, and the second is the expansion of the concentrate along the strip. The first step is to avoid chaos or return to disaster, as Arif suggests [6]. The final process for obtaining a uniform concentration distribution is a complete symbol of mixing, which is achieved by molecular distribution (the second method).

Nevertheless, the correct structure of the hidden size is a precondition for rapid heating, and this cannot be achieved without the aid of a sieve.

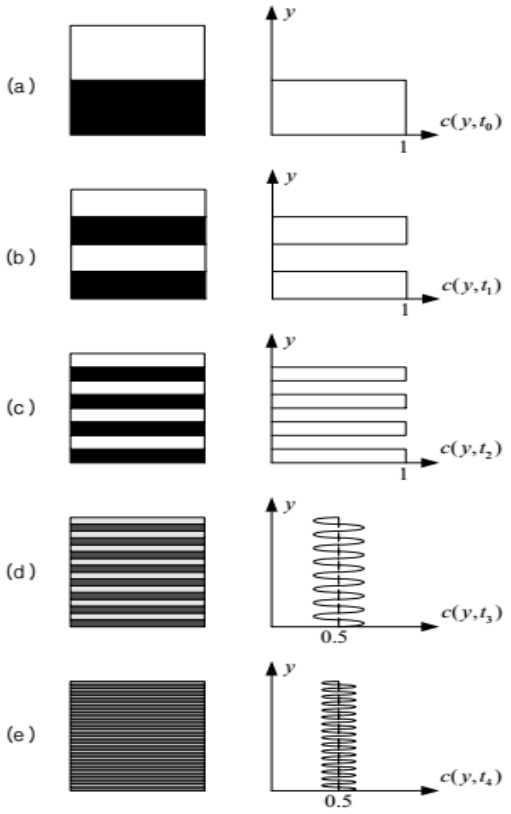

Figure 5: Development of a stratification pattern (a) to (c) smooth (d) chaotic

1.2 Various Mixer Designs for Microfluidic Applications

Now, let us look at the different views on microfluidic mixers that have been reported since 2005. Referring to the literature, we see that many articles discuss the flow of media or high Reynolds numbers. However, we do not include these papers in this analysis because the medium or elevated Reynolds number flow rate is seldom institute in these applications. With such a flow, it may be easier to attract an unstable and complex flow that naturally plays an important role in the synthesis of liquids.

Micro fluidic mixers can be dispensed in different ways. In this article, we use the class bodily mechanism. They focus on hydrodynamic, alternative injections, engineering effects, electrophoresis, drop mixing and particle syringes.

1.2.1 Hydrodynamic Focusing

The primary method of hydrodynamic concentration is presented in Section 2. [8] Formation of a small silicon channel with 10 inlets for dissolving acid and alkaline solution (see 6). By comparing the measurements of their mixed performance experience with computer flow dynamics (CFD) results, they are consistent at the time of residence. Nguyen and Huang [9] proposed a comparison of the measured value of the analytical solution in the hydrodynamic concentration device and the experimental spread of the sample. He gained attention by using a pair of bridge channels. The uniqueness of their research is that they increase the response to an increase in the pulse of salt in the channel. In this design, the inlet valves are created by two boards of Pico electric valves. This article mentions that Taylor can improve the spread. Edison and Lowell [10, 11] introduced the well-known multi-layer micro mixer long for mixing two flow samples (Figure 7). Its design consists of a number of hybrid structures strategically placed under the mixer channel, in which the blocks are wonderfully arranged internally. The results show that fluid transfer and lengthening methods are most effective in increasing mass transfer. Cha et al. [13] He proposed a small 3D mixer that combines the functions of concentration and tomographic re amalgamation (SAR), called the Bast Mixer (Figure 8). For a flow rate of 12.7 µl / min, only 90 mixtures are found in 1.4mm. Park et al. [13] The use of meridian stimulation by hydrodynamic concentration proved to be an effective way to control the sample response. They created five internal channels: the analytical solution center, the solution B dimensions, and the solution a disturbance. In this way, they can avoid the unwanted solution from being primed before the concentration is completed. The vascular system mimicked the engineering B.O., Sicilian and Pechna [14] designed the branch channel and studied the mixed function of numbers, with a particular focus on the effect of branch counting.

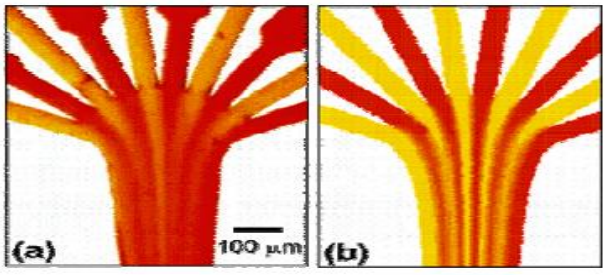

Figure 6:Mixing of Fluid (a) experimental (b) Simulation.

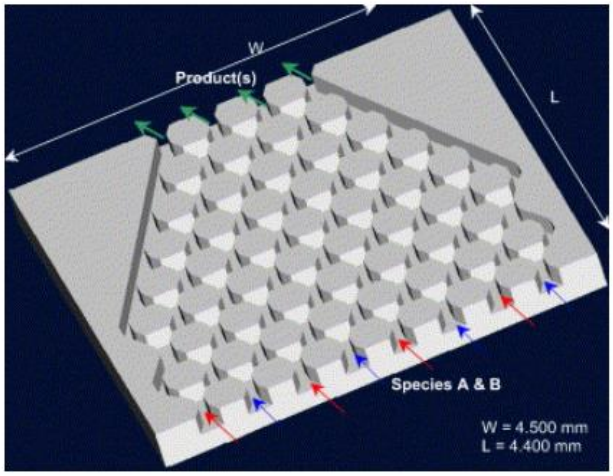

Figure 7: Multi-laminated flow mixer

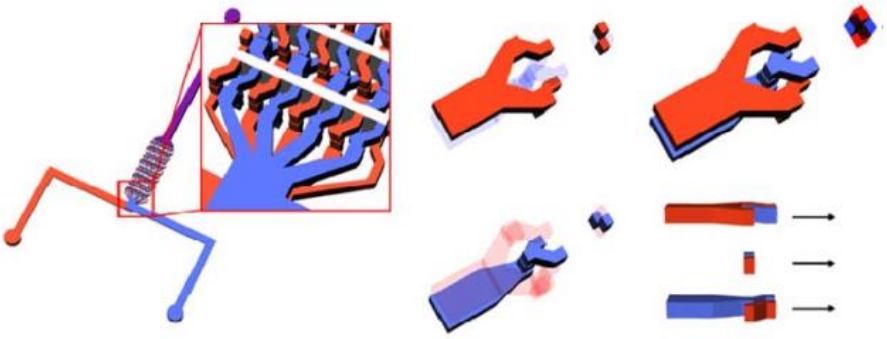

Figure 8: Representation of chess board mixer

1.2.2 Alternate-Injection

Another popular way to improve the efficiency of a mix is to put different types of samples inside the mixture separately. In the R.A. of each sample, the flow is same as a pulse. Compared to the hydrodynamic concentration case, the alternative injection strategy does not necessitate intricate channel construction. Numerical and analytical studies have been performed on the differential performance of two dissimilar models hosted to the channel by the mechanics and [15] pulse pressure. This increases the area of the alternative injection interface, resulting in faster synthesis. Goltt et al. [16] reviewed the effect of input channel geometry (e.g., "T" and "Y", etc.) and the phase variance in injected testers on the pulse flow mixer mixing function. They inserted ribs into the central canal and showed significant enhancement in the extent of mixing.

As a dynamic force for sample injection, electrosomes are much more useful than pressure. The Hunton Research Group [17, 18] led an investigational study on the effects of mixing in cross-inlet channel and large mixing tent tube design, in which samples were injected by electrical force, respectively. The slow flow line in the extension duct is connected to the lawn thinner and thinner, thus increasing the distribution. The results show that in specific parameter settings, the optimal frequency of the optimal combination is in the range of 1-2 Hz. Living Eight offered a similar design. [19] and Sun and C [20].

The hypothesis of easy replacement injection can be enhanced or changed for better mixing. Fu and Sisai [21] proposed the customary name of numbers for fluid concentration alternately through simple double "T" and "T" channels. They showed that, compared to a “T” design, twice the “T” channel provides a faster mixing effect (Fig. 10). In the work of Lee et al. [22], under the conditions of nine-linear dynamics, such as Liponov AC and Pioncara part reaction, the defective contacts entering the mixer were analyzed in detail. When injecting the liquid through the side channel, they showed that the liquid has the maximum injection frequency to obtain the maximum mixture. In Chen and Chou's work [23], in supplement to the injection of plastering liquid through the inner canal, the main canal wall was also designed to allow separate separation patterns to pass through the drawing layer which leads to the mixing process promotes effect (fig.11)

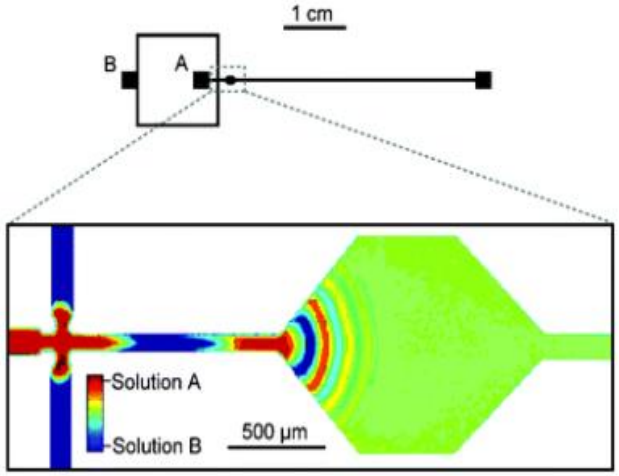

Figure 9: Alternate-injector mixer composed of compressed air.

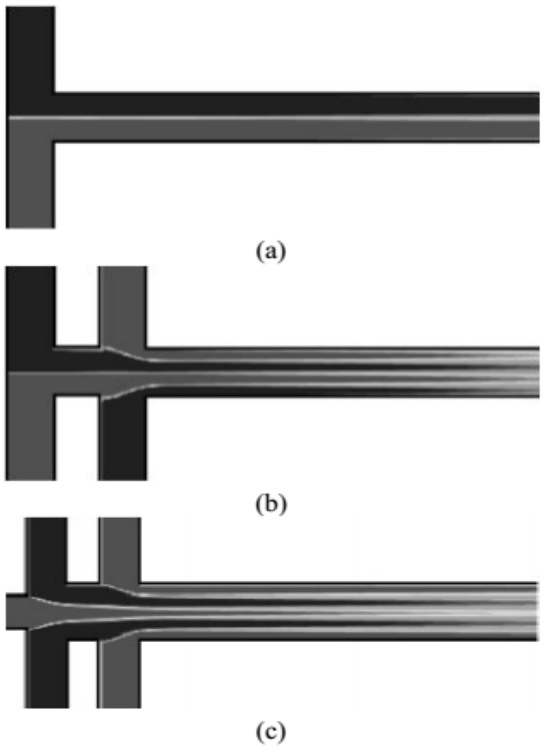

Figure 10: Inlet passage (a) Single T (b) Double (c) X-cross channel

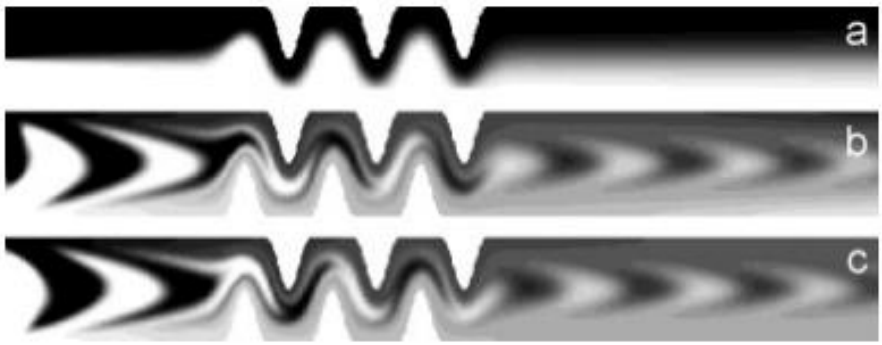

Figure 11: Wavy wall channel having (a) Continuous (b) Pulsed (c) pulsed with double period.

Like the hydrodynamic concentration technique, the AC injection technique also has major disadvantages. The return is only in the inner area of the channel. The larger room, however, is associated with the proposed intake passage of the Hunton Group [17,18], Leont Out. [19] and Sun and CE [20] increase the mixture through large expansion, which is the opposite of chaos prevention, as this expansion only occurs over time. In addition, when electromagnetic force is

used to inject liquids due to their usefulness in controlling injectors, bubbles created due to electrode failure or damage may cause another problem. Therefore, for practical use, it is necessary to solve these problems.

1.2.3 Effect of Geometry

Obviously, the easiest way to improve the synthesis in a non-channel is to make the channel a geometric complex, for example, a narrow wall [24], a groove [25] or a block in the lower wall [26]. Less [27] projected a smaller two-layer duct consisting of a series of F-shaped channel units (Fig. 12), which exhibits a disturbance through the expansion mechanism. Chia and others. [28] Compare the mixed effects of two cross-channels with two layers, including the first snake mixer anticipated by Liu et al. [24] See Figure 13. Below the lower Reynolds numbers, their two design types (Figure 13a and 13b) show better synthesis presentation than the serpentine housing (Fig. 13c), meaning that the lower Reynolds is not suitable for small serpentine housing channels. The Ansari influence by the flow of numbers is Ansari and few [29] support this theory. The two-stage structure is proposed by Jan Ott. [27]. Wuchia et al. [2] showed emotional turmoil, but the main drawback of these constructions is once again that the creation of two separate comparisons would surge the cost of the device. Howell et al. [30] anticipated a two-layer design not only on the bottom, but also on the upper wall with serious lines and grooves. Its design only combines faster than a container [25], but here again the production difficulties should be eliminated as it has proven useful for practical applications. Similarly, Yang and so on. [31] It was suggested to make a circle on the upper wall in addition to the lower duct to carry the liquid closer to the upper wall, but this duct may not be so easy to make.

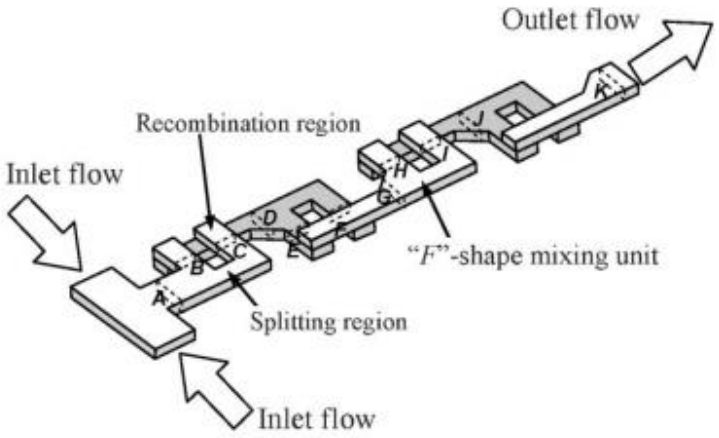

Figure 12: Laminated mixer with serpentine arrangement

As a mono unsaturated structure, the mixer anticipated by Cement and Grovesman [32] deserves our attention. Its design consists of a compound but single layer of PDMS (polydimethylsulosin) attached to the flat upper wall (Fig. 15). As shown in Figure 15, the apparent analysis causes confusion in the duct. When two samples are presented in the upper and lower regions of the channel segment, the proposed design shows the best effects of the mixture, but this means that there is no interest when entering the left domains. To shorten the mixing time, Kamaska et al. [33] He presented a sample of the water factory at the end of the canal (Figure 16).

The wire trace function is used in pattern design where D is one of the key constraints. It was discovered that reliant on the D, mixing may be better than the unique Straw ET. [25]. However, even if a chaotic mix is seen in the upper region of the drain, it is still a problem because there is a current close to the upper region. The lower canal is somewhat connected to the wall. Numerous changes to the trench channel design have been tested. Young At [34] In addition to the low-capacity duct by stroke and others. A side drain is also designed. [25] For the second flow increase (Fig. 17) it was found that the presence of tubes improved the efficiency of the mixture by 10-50.

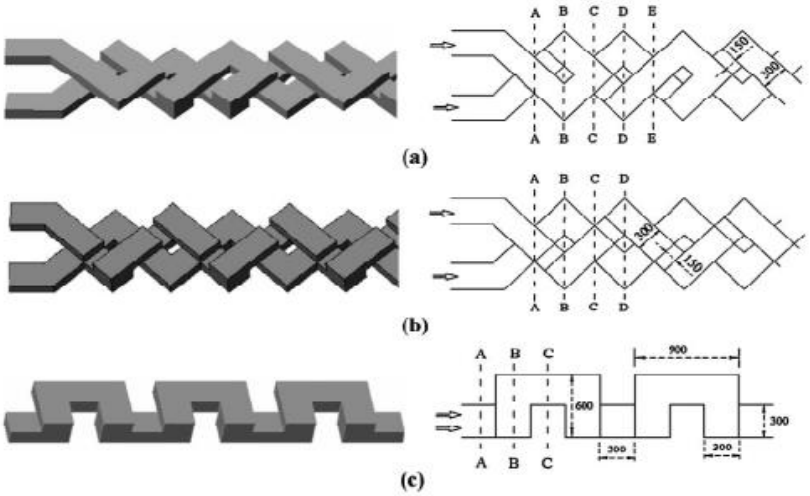

Figure 13: Three kinds of micro channels with multi layers

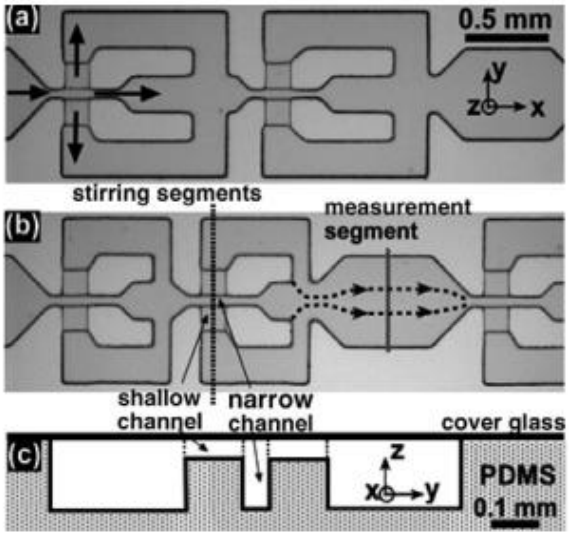

Figure 14: (a)-(b) Single layer of structure (c) Section view of sectional plane of channel mixer

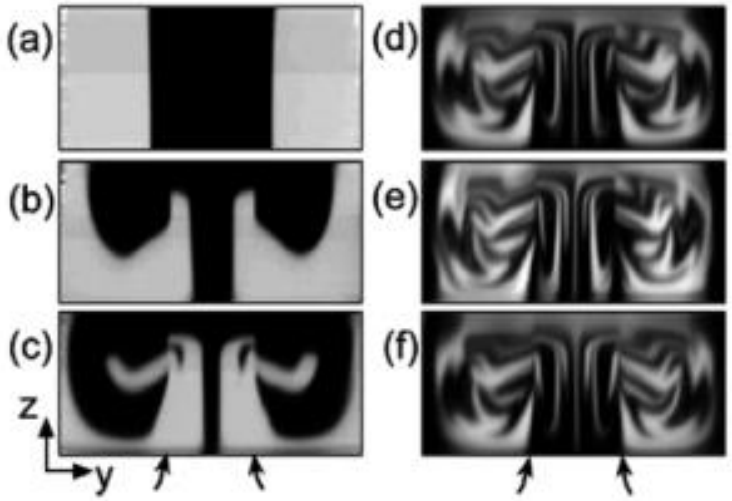

Figure 15: Development of pattern inside a channel

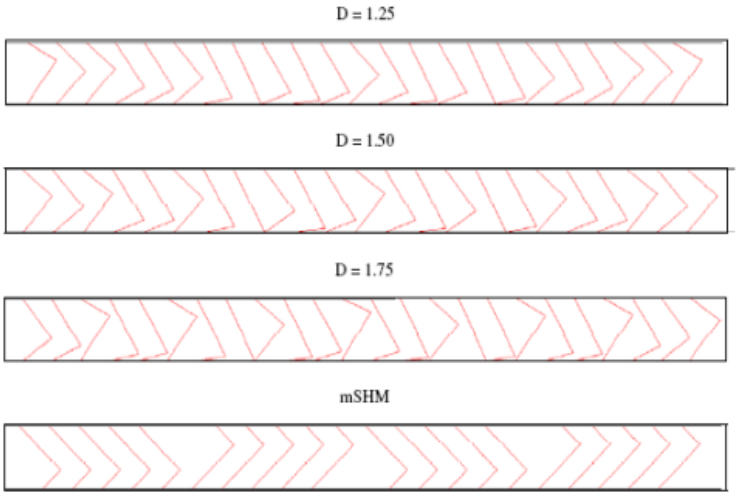

Figure 16: Top view of fractal pattering of grooves.

The design ID for the SR comes directly from the measurement method for seamless transmission. The literature [35] described investigational and algebraic outcomes of hybrid activity in SAR design, mirroring the original concepts of fold expansion patterns in chaos (Fowler 18). Compared to the mapped design on the bottom wall, this design can ensure uniform mixed properties along the channel cross section. Of course, the problem is the production of problems. Lee et al. [36] Steps and sections are proposed to be used in the first wall of the canal (Fig. 19) to create a separation and repair function, and there is no central trouble in the preparation progression. Seven more. [37] They also proposed a new canal design consisting of several black heads. Indication of the effect of folding can be clearly seen from the numbers and the experimental style (Fig. 20).

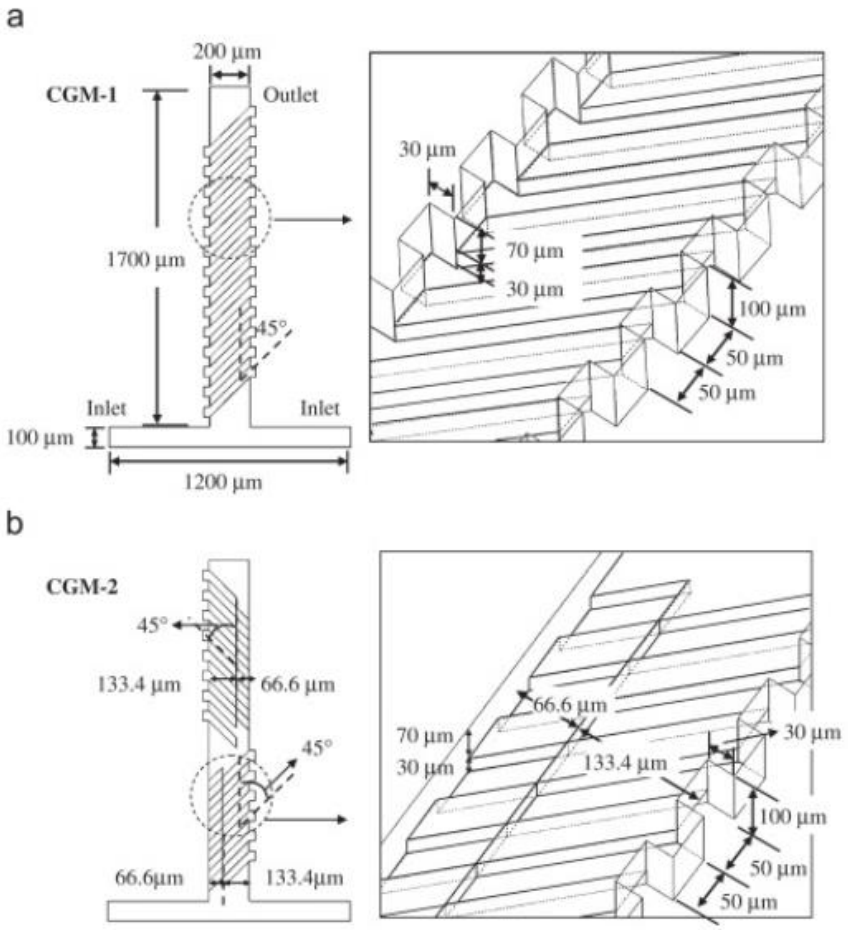

Figure 17: (a) CGM-l Design (b) CGM-2 Design

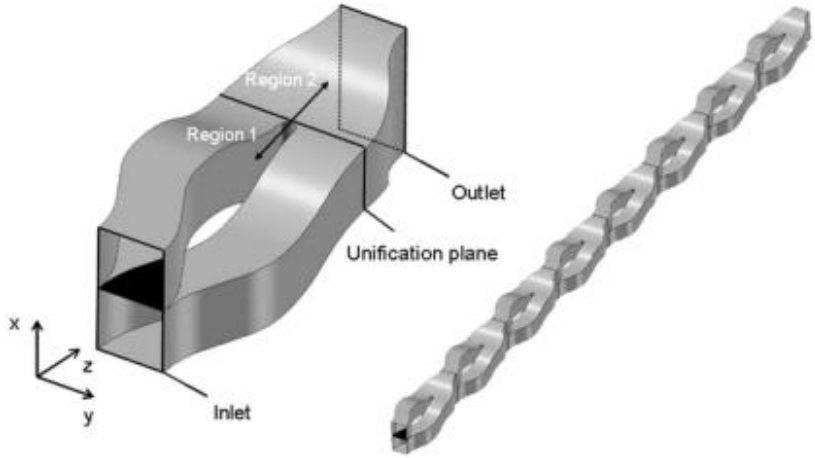

Figure 18: SAR unit enlarged view.

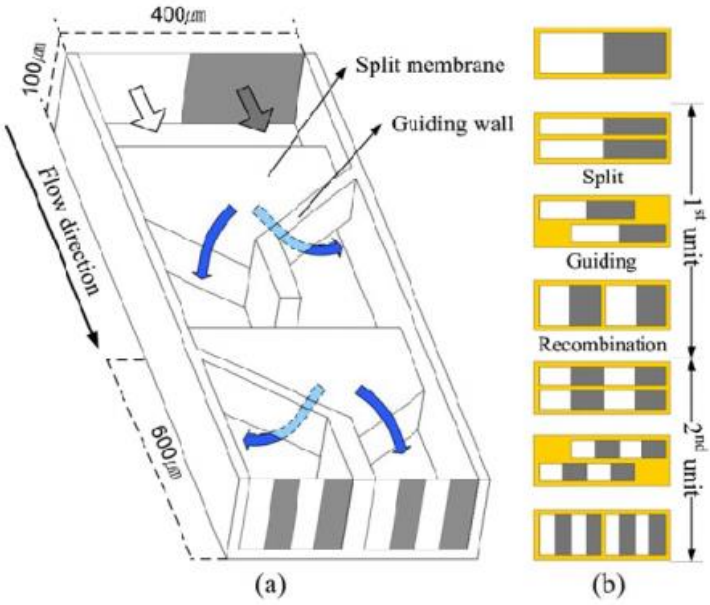

Figure 19: (a) SAR mixer with steps (b) Mixing of in SAR module.

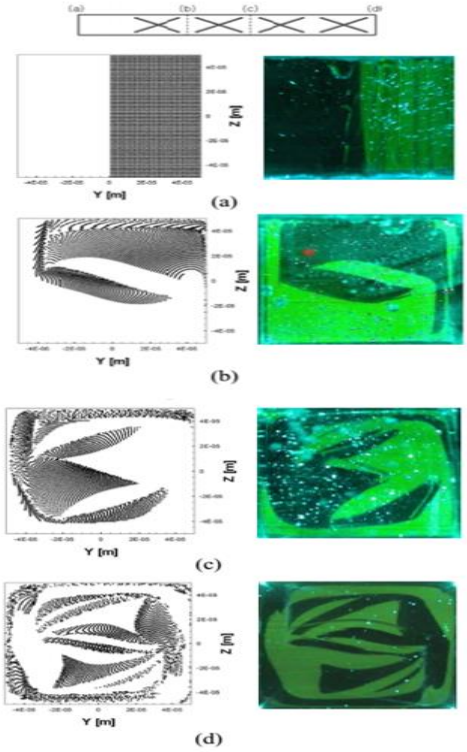

Figure 20: Comparing of patterns from numerical to experimental.

1.2.4 Electro-kinetic Method

The electrostatic effect, especially electric whitening, is not only an effective tool for pumping liquids, but also an effective tool for controlling liquid flow, which is crucial for mixing liquids. In Section 3.2, we discuss several studies that have used electric current as a method to convert liquid injection through a method channel. In this section, we present a study of local flow control and its effects on synthesis.

First, we distribute the zeta capacitance in the channel wall. Cheng et al. [38] offered a numerical study of fluid flow and analysis in a 2D channel, side walls that determine physically different zeta capacities. The results show that this potential distribution of different fats can lead to more complex flow patterns, which improves synthesis. In the work of Chen and Cho [39], the effects of additional wave walls were also studied. Zeta capacity in a section of channel wall can be controlled in the following ways:

Processing technology. On the other hand, this can only be created by placing the connector on the wall.

Experimental and numerical studies of local eddy series such as Wu and Lee [40]. Unlike an insulated wall, the surface of the conductor wall is kept at the same voltage, so an uneven distribution of the power field near the insulating piece will cause a local base, which can be used for mixing (Data. 21). In Kang. [1] Using the L-Boltzmann number method with the use of number 2D and 3D micro-channels with different zeta extensions, these channels change or persist over time. They verified by linking their consequences with the digital codes provided by the business code for the 3D channel. Adjustment is the ideal period of regulation to maximize changes in zeta capacities over time.

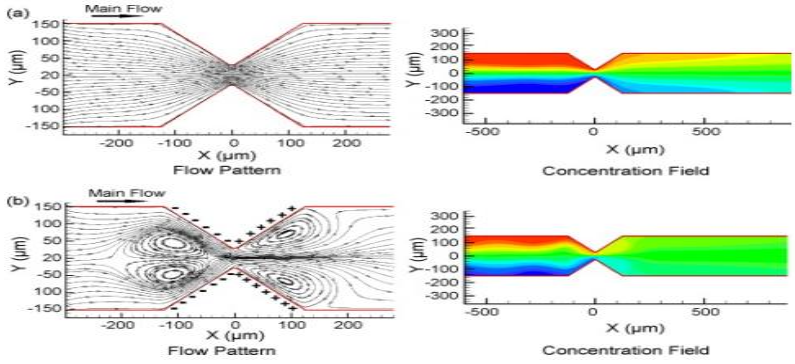

Figure 21: (a) Non conducting (b) conducting hurdles flow contour.

The development of micro-channel electrodes has attracted public attention, as they use wall-mounted electrodes or have direct contact with fluids to control the flow and synthesis of fluids. Kian and Bao [2] showed a disturbance in the rectangular bore that from time to time caused the electric saucers to operate at different slate speeds in the upper and lower walls. They performed 2D numerical mapping to obtain Poincar cross sections using a Stokes flow semi-analytical solution during coffee. Zeta capacitance that changes in the wall section over time can be achieved by adjusting the voltage applied to the electrode under the wall section. Xiao and Bao [43] proposed a two-dimensional study of color mixing. Chaos can be achieved temporarily by regulating the distribution of electrical inequalities at the inner wall surface. Wu and Liu [44] believe that there are electrodes in the wall below the embedded channel under the T-shaped channel in Chevron (Fig. 22). It was found that the use of zeta voltage control using combined electrodes can greatly amplify the mixing effect. Sasaki et al. [45] Experimental evidence (Figure 23) proved that the effect of a mixture is amplified by a pair of dissolved electrodes in the "Y" channel (Fig. 23), and that the current is moving competitively. The electric pair Huang It tried to use more complex micro-electrode patterns on the canal walls [46]. More Enhancing the effect of the mixture is shown in (Fig. 24).

The use of micro-electrodes makes it easier to control local methods (such as pressure-based flow) than other methods. However, without saying that this additional equipment increases the cost of precision equipment. In addition, the application should be limited to incentive fluids.

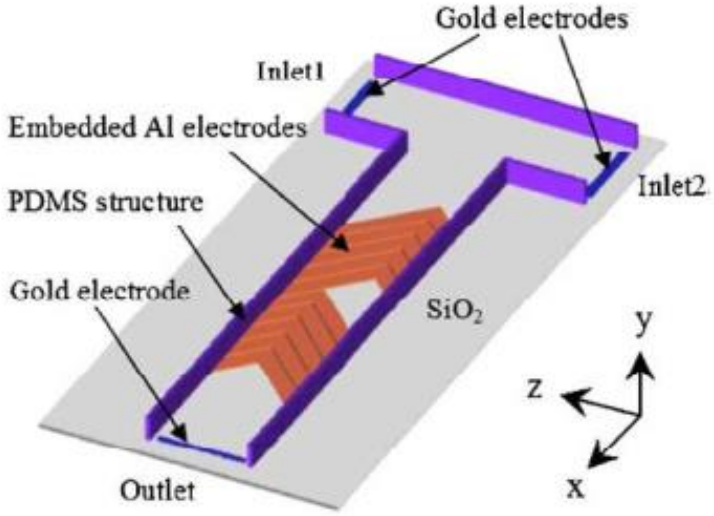

Figure 22: T typical micro channel

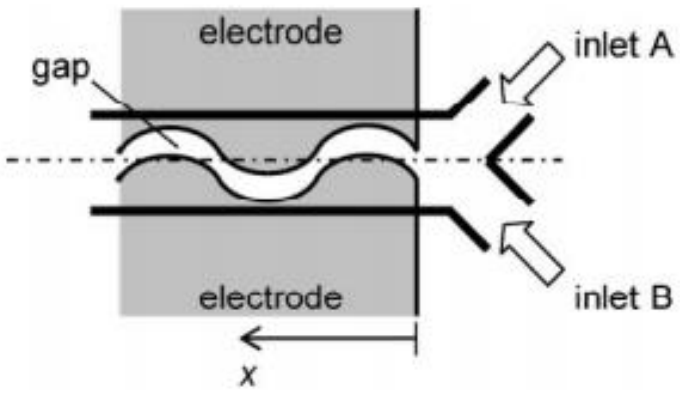

Figure 23: Y shape micro channel

Hybrid adjustment can also be achieved through electrodynamic or physicochemical instability. For example, Green and others. [47] showed an experimental research on the variability of electrical motion and its use in mixtures. The introduction of NaCl solutions of separate absorptions will create a gradual increase in transport performance in the interface, and thus create costs. This distribution of compensation, combined with a variable external electric field, encourages electromagnetic instability (Fig. 25), which is cast-off as a dynamic mechanism for increasing the alloy in the duct path. It was found that the maximum frequency for mixing is twice the natural frequency of electrical energy instability. Thyl [48] proposed an experimental learning of a very fast mixer in which ion consumption was used and they were replaced with an electric field enriched close to a poly-electric gel, thus giving rise to spot charges. The results show that the effect of mixing is desirable, and the mixing has a maximum frequency. He successfully used his determination in the blood cells. However, only when two mixed interfaces exhibit electro-kinetic instability after mixing mainly due to the difference in concentration, mixing by this method can be effective.

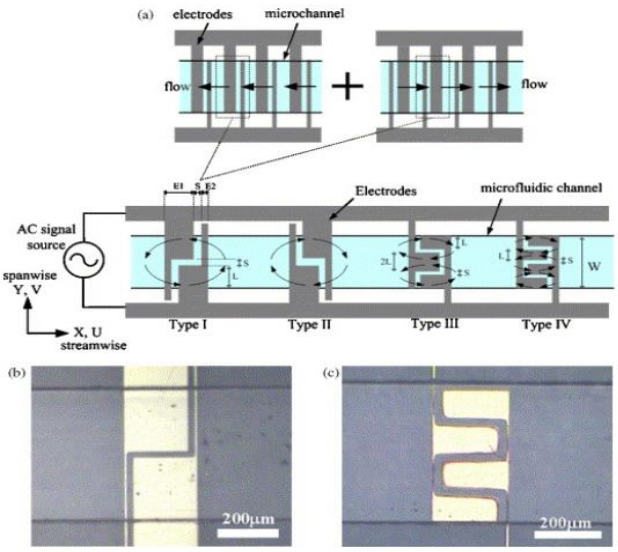

Figure 24: (a) Electrode pattering for vortices (b) (c) Design I and IV

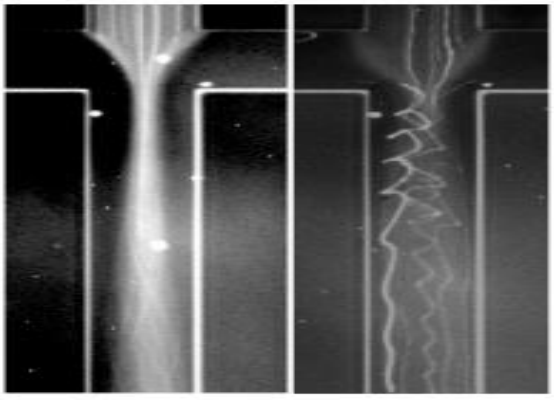

Figure 25: Particle flow pattern in static and transient electrical fields

1.2.5 Mixing by formed droplets.

Pressure-driven currents are often used in constant flow mixers, such as hydrodynamic concentration, alternative injection, or geometry shifting techniques, due to the dissipation of equal velocities that must be widely distributed over a lifetime. "To eliminate this problem, droplets or lumps have grown. Due to the strong surface pressure at the surface between the sample (which has a droplet) and the transporter fluid (usually fat), the droplets are always in a separate bin. Such as a finite ball or cylinder. Therefore, each liquid particle must be reduced to the same residence time. An additional advantage of droplet mixing is that the flow essential for mixing can be produced comparatively easily through authorized channels.

Liao et al. [49] designed a gable canal with defects on the outer side of the curved portion (Figure 26). This design balances the inner flow of the pole further than the bulge because the oil layer on one side of the bulge Is appropriate. The sides are really sharp, resulting in a lot of working fluid shadow pressure towards the bulge. Muradoglu and Potter [50 51] created a 2D numerical map of the composition mix within the drop channel. The results show that when the droplet size is equal to the channel width, the best mixing effect can be achieved. The effect of the number of capillaries is significant. The less cashier, the better the mix. The ratio of adhesive droplets to the surrounding liquid should be as low as possible to obtain the best composition. Tung and colleagues studied the effects of channel geometry on droplet mixing [51]. Oil, a small snake-like channel as a shipper liquid, was proposed by Dr. Gan et al. [52] an accepted channel uses gas as the carrier current. In the last study, when the angle of contact is less than 90, the gas is in a fast cylinder instead of a liquid. What the two studies have in common with other studies on this issue is that they identify an ideal channel configuration for rapid mixing rates in individual design.

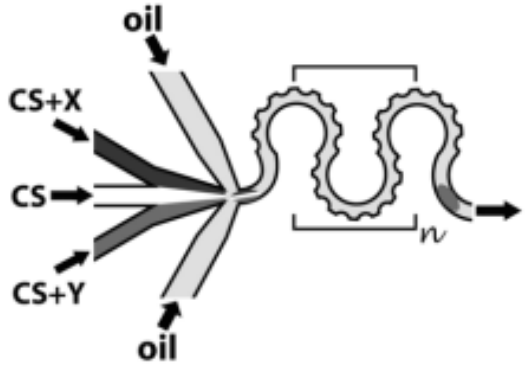

Figure 26: Meandering channel with bumps

When estimating the efficiency of compound mixing based on the material concentration distribution, attention must be paid to the concentration distribution in the initial conditions. In work of Tanthapanichakun and others [53] It was revealed in the statistics that the initial concentration was the most important factor influencing the rate of disturbance, which was also noted in the work of Wang Atal. [54]. This resources that the flow area is called the drop-down area. Sarah, Sarzan and others for research on such issues. [55] Two different methods of abortion are considered.

Mixing, that is, linear management and side-by-side management as shown in Figure 27, droplet fusion with long-term regulation provides a better synthesis effect, according to a study by

Tantapanichakoon et al. [53] and Wang et al [54]. Liquid oil is often used as a carrier. Rheumatism and combustion, on the other hand, use air as a carrier flood (Fig. 28). They were able to create separate goosebumps in the micro-channels and use the current driven by the relative movement of the channel walls to achieve better synthesis. The drops are said to remain without falling off the wall.

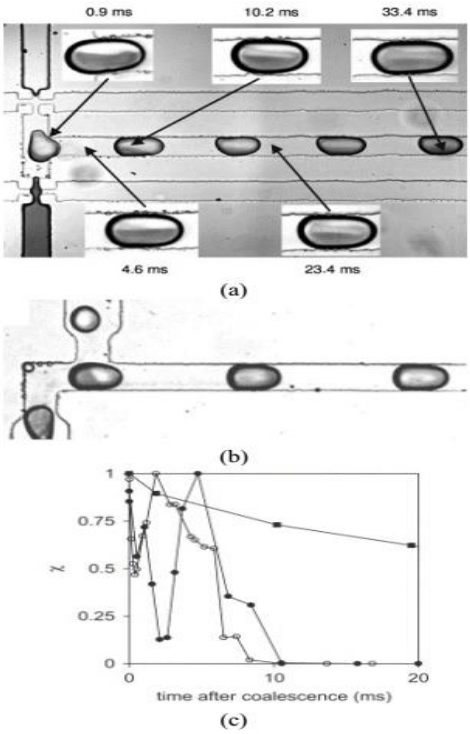

Figure 27: Droplet sticking (a) Parallel (b) Longitudinal.

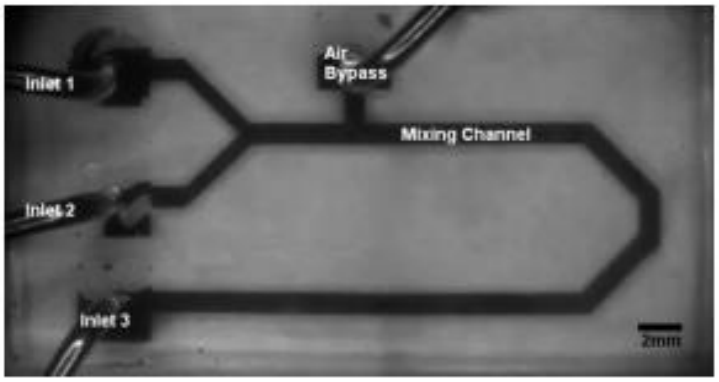

Figure 28: Micro mixer with an air inlet port

The condition of using droplet mixing is that the hauler liquid and the target sample must not be mixed. Typically, the sample contains water, so it is easy to find a carrier liquid such as oil. When the droplet interface completely touches the channel wall and the interface leftovers flat, the reaction result can be easily observed without compromising the image quality. In this case, the branch is called "Gabes". Currently, there are no major drawbacks to the method of mixing drops.

1.2.6 Stirring by Particles

Typically, liquid agitation is used with magnetic particles to mix the liquid in a precision device. Grumman et al. [57] The mixing chamber, approximately 6 mm in diameter, contains 68 μm electromagnetic balls rotating on a fixed disk, and the permanent magnets are radially distributed on the hard disk, so the magnetic particles realize the time and diameter of the chamber and move towards the waves. It has been found that the magnetic field, which changes over time, improves mixing, and substituting the path of rotation improves the mixing speed. It is identified that when a magnetic field is functional to a liquid comprising dispersed paramagnetic particles, it tends to form chains (see [58-60]). Obviously, when agitating the stirring fluid, the linear structure of the particles should be more efficient than the individual particles. Calhoun et al. [61] focused on performing simulations of a two-dimensional Boltzmann network using a dipole model that improved fluid mixing due to revolving chains of paramagnetic particles. It has been found that proper repetition of grinding and deformation is essential for optimal mixing. Franke and colleagues [62] also confirmed the possibility of using rotating magnets and magnetic circuits to move liquids in their experiments. Lee et al. [63-64]; The first study used super magnetic particles, and the second study used ferromagnetic particles. Roy et al. Even in micron-sized droplets, a magnetic field can effectively agitate the liquid for mixing, as in a large batch mixer. There is an ideal build number (mucilage percentage) for better mixing. Lu et al. Literature [65] executed numerical simulations of mixing and motion of fluid in microchannel, and this process occurs due to the motion of magnetic particles caused by a magnetic field that changes over time. It has been proven that there is an optimal magnetic field modulation period for optimal mixing. Intriguingly, the grouped particles form separate bodies flowing around them.

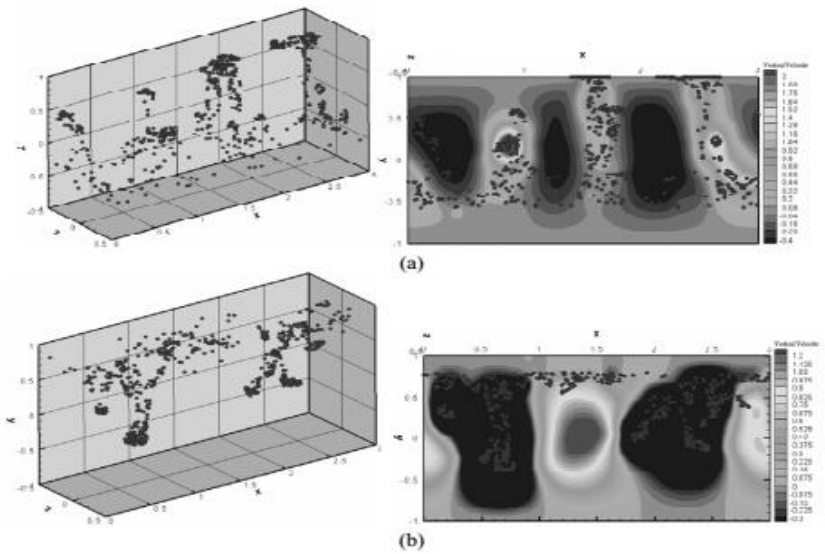

Figure 29: Magnetic particles distribution in (a) half period (b) full period

1.3 Problem statement

The mixing in the microchannel is highly dependent on various parameters. This study focuses on the enhancement of the mixing through passive means. A sinusoidal, time dependent temperature variation is applied on the upper and lower walls of the channel. The waves travel in opposite direction to each other. This study focuses on the effects of the wavelength on various parameters involved in microfluidic mixing.

1.3.1 Project objectives

Following are the objectives of the project.

(a) Validation of the computation model by comparison with published data.
(b) Study of various parameters dependency on wavelength of temperature waves.
(c) To determine the nondimensional number U_{th}/U, h/ δth and Prandtl number.
(d) To study the effects of wavelength variation on vorticity and mixing enhancement.
(e) To study the effects of wavelength, change on Reynold and Strouhal number.
(f) Mixing enhancement by TVEC effect at very low Reynolds number.

CHAPTER 2: METHODOLOGY

Before proceeding to the CFD analysis part, the mathematical model of micro mixer needs to be established. Details of mathematical as well as simulation model along with boundary conditions are as follows.

2.1 Mathematical modelling

In case of a constant Reynolds number, mixing efficiency of channels with a high-level aspect ratio of rectangular cross section is advanced as compared with lower aspect ratios because of the greater contact surface area. Therefore, generally 2D microchannel are analyzed. However, extending the results to 3D is interesting and beneficial. The geometry studied here is a simple two-dimensional channel shown in Figure 30. Two mismatch states of the boundary in the form of a sinusoidal temperature varying wave propagating in opposite directions imposed on the walls of the opposite channel, and each channel wall is characterized by three parameters: wavelength λ and wave velocity v_{th} amplitude ΔT. This study assumes that these two waves are same. It should be noted that the range of fluctuations of these parameters is a rather technical issue. Therefore, the thermal boundary condition of a small channel is expressed as:

$$T = T_0 + \Delta T \sin\left(\frac{1}{\lambda}(2\Pi x_1 + i t v_{th.})\right), \begin{cases} i = -1, & if x_2 = h \\ i = +1, & if x_2 = 0 \end{cases} \quad (1)$$

Governing equations of mass, energy and momentum are as follows.

$$\frac{Dp}{Dt} + \rho \vec{\nabla}.\vec{V} = 0 \quad (2)$$

$$\rho\left[\frac{\partial \vec{V}}{\partial t} + (\vec{V}.\ \vec{\nabla})\vec{V}\right] = -\vec{\nabla}p + \frac{\partial}{\partial x_k}\left\{\mu\left[\left(\frac{\partial v_l}{\partial x_k} + \frac{\partial v_k}{\partial x_l}\right) - \frac{2}{3}\delta_{kl}\vec{\nabla}.\vec{V}\right]\right\} \qquad k, l=1,2 \quad (3)$$

$$\rho c_p \frac{DT}{Dt} = \alpha_T T \frac{Dp}{Dt} + \vec{\nabla}.\left(k\vec{\nabla}T\right) + \Phi \quad (4)$$

The density in equation (4) can be defined as

$$\rho = \rho_0[1-\alpha_T(T-T_0)] \tag{5}$$

Thus, final form of conservation equation becomes by putting in equation (2)

$$-\rho_0\alpha_T\frac{DT}{Dt} + \rho_0[1-\alpha_T(T-T_0)\vec{\nabla}.\vec{V} = 0 \tag{6}$$

Presuming that differential pressure is zero resulting in that considering pressure work and viscid dissipation is unimportant in energy equation so by disregarding these terms and making linear we have.

$$\vec{\nabla}.\vec{V} = \alpha_T\frac{\partial T}{\partial t} \tag{7}$$

Which indicates that when temperature fluctuates by thermal waves this equation fluctuates regularly. We can also get the periodic velocity field of the fluid by this equation.

If we consider that hydrodynamic and thermal penetration length scale is identical then we can say that δth is the length scale in perpendicular way

$$\delta_{th} = \left(\frac{\alpha_0\lambda}{v_{th}}\right)^{\frac{1}{2}} \tag{8}$$

Where $\alpha_0 = \frac{k_0}{\rho_0 c_p(T_0)}$ is the diffusivity of the temperature in the fluid whose value is 1.47×10^{-7} m^2/s.

Assuming the change of pressure with domain is

$$p(x_1,x_2,t) = -\frac{\Delta p}{\lambda}x_1 + p'(x_1,x_2,t) \tag{9}$$

In this equation Δp is the differential pressure per each wavelength while p' is the small pressure field which is produced by the imposed thermal waves across the walls.

Viscosity changes with temperature as the fluid is dependent on the temperature change so viscosity changes as follows.

$$\mu = \mu_0\left[1-\eta_T\left(T-T_0\right)\right] \qquad (10)$$

Putting equation (9) & (10) in dimensionless momentum equation along the microchannel length we obtain

$$\frac{1}{\mathrm{Pr}}\left(\frac{h}{\delta th.}\right)^2\frac{\partial v_1^*}{\partial t^*} = \frac{\Delta p h^2}{U\lambda\mu_0} + \frac{\partial_2 v_1^*}{\partial x_2^{*2}} - \eta_T\Delta T\frac{h}{\delta th.}\frac{\partial\theta\partial v_1^*}{\partial x_2^{*2}} - \eta_T\Delta T\theta\frac{\partial^2 v_1^*}{\partial x_2^{*2}}$$
$$-\left(\frac{h}{\lambda}\right)\left[\frac{\varepsilon\Delta p h}{U\mu_0}\frac{\partial p'^*}{\partial x_1^*}\right] + 2\left(\frac{h}{\lambda}\right)^2\left[(1-\eta_T\Delta T\theta)\frac{\partial}{\partial x_2^*}\left(\frac{\partial v_2^*}{\partial x_1^*}\right)\right]$$
$$-\eta_T\Delta T\frac{h}{\delta th.}\frac{\partial\theta}{\partial x_2^*}\frac{\partial v_2^*}{\partial x_1^*} + \frac{\partial^2 v_1^*}{\partial x_1^{*2}} - \eta_T\Delta T\frac{\partial}{\partial x_1^*}\left(\theta\frac{\partial v_1^*}{\partial x_1^*}\right)$$
$$-\frac{1}{3}\frac{\alpha_T\Delta v_{th.}}{U}\frac{\partial}{\partial x_1^*}\left(\frac{\partial\theta}{\partial t^*}\right) + \frac{1}{3}\frac{\alpha_T\eta_T(\Delta T)^2 v_{th.}}{U}\frac{\partial}{\partial x_1^*}\left(\theta\frac{\partial\theta}{\partial t^*}\right)\Bigg] \qquad (11)$$

For thin micro channels, the upper equation reduces to

$$\frac{1}{\mathrm{Pr}}\left(\frac{h}{\delta th.}\right)^2\frac{\partial v_1^*}{\partial t^*} - \frac{\partial^2 v_1^*}{\partial x_2^{*2}} + \eta_T\Delta T\left(\frac{h}{\delta th.}\frac{\partial\theta\partial v_1^*}{\partial x_2^{*2}} + \theta\frac{\partial^2 v_1^*}{\partial x_2^{*2}}\right) = \frac{\Delta p h^2/\lambda\mu_0}{U} \qquad (12)$$

If we assume that TVEC effect is absent than equation (12) would change in to

$U_{pois.}$= $\Delta p h^2/12\lambda\mu_0$ which show that average axial velocity of flow is happening there.

Total average velocity of flow is calculated by sum of U_{th} and $U_{pois.}$.

Thus non –dimensional number for the analysis are described as

$$\frac{U_{th}}{U} = \frac{\alpha_T\Delta T v_{th.}}{\alpha_T\Delta T v_{th.} + h^2\Delta p/12\mu_0\lambda}, \frac{h}{\delta th.} = \frac{h}{\sqrt{\alpha 0\lambda/v_{th}}}, Pr = \frac{\delta 0}{\alpha 0} \qquad (13)$$

2.1.1 Effects of Strouhal number on chaotic mixing for various values of λ.

When a fluid chunk undergoes fluid rotation in micro channel the relaxation time is given by

$$t_{rel.} = \frac{\lambda}{U_{pois.}} = \frac{12\mu_0\lambda^2}{h^2\Delta} \tag{14}$$

The Strouhal number can thus be defined as

$$S_t = \omega t_{rel.} = \frac{\omega\lambda}{U_{Pois.}} = \frac{12\mu_0 v_{th.}\lambda}{\Delta p h^2} \tag{15}$$

And relationship of ReSt can be defined as

$$\frac{1}{\Pr}\left(\frac{h}{\delta_{th.}}\right)^2 = \frac{h}{\lambda}\mathrm{Re}\,St \tag{16}$$

Whereas $\mathrm{Re} = \frac{U_{pois}*h}{v_0}$

It can be seen form the equation 13 that the ReSt is independent of Δp and ΔT. So, from this expression we can say that when Re increments with differential pressure than with same ratio St experiences drop resulting is that TVEC effect falls and chaotic mixing will not be achieved. Relatively speaking if we put Δp=0 which means Re is also zero but St →∞ and resulting in homogeneously mixing. Conversely if we presume as Δp→0 which means Re also approaches to infinity, but the St experiences drop which approaches to zero resulting in almost nil mixing. From these results we reach to the conclusion that there occurs a narrow scale among which chaotic mixing can be attained realistically

2.1.2 Vorticity effects on chaotic mixing for various values of λ

Vorticity of the microchannel fluid is a result of constant overlapping and stretching of the deformed fluid interfaces. If the thickness of the fluid element is decreased, then the magnitude of the gradient perpendicular to the face are increased. Thus, more diffusion takes place. In 2D channel vorticity and strain rate can be defined as

$$\xi(x_1, x_2, t) = \frac{\partial v_2}{dx_1} - \frac{\partial v_1}{dx_2} \tag{17}$$

$$s(x_1, x_2, t) = \frac{1}{2}\left(\frac{\partial v_2}{\partial x_1} + \frac{\partial v_1}{\partial x_2}\right) \tag{18}$$

If we adopt ΔP = ∞ then engulfment of one domain on another does not occur as because of flow which is only a Poiseuille flow due to non-serviceable TVEC effect, for that situation we can conclude s = -1/2 ξ which shows these prompts the stretching in fluid motion is happening but not engulfment which is well-thought-out as primary phase of the stirring [68]. So, if these both vorticity and strain rate follow elevation with Δp no enhancement in mixing will be achieved due to nonappearance of engulfment. In other words, differential pressure does drive the fluid in micro channel, then the fluid is stirred by expansion and contraction under thermal waves which depend on lambda. So, vorticity is the thing which shows both elongating and engulfment. Thus, if suitable value of ΔP is selected high stir values can be achieved.

The dimensionless mean vorticity is thus given by.

$$\bar{\xi}^{*}(t) = \frac{\bar{\xi}(t)h}{U} \tag{19}$$

And mean vorticity can be calculated on basis of following equation,

$$\bar{\xi}(t) = \frac{1}{A}\int \sqrt{\xi^2(x_1, x_2, t)}\, dA \tag{20}$$

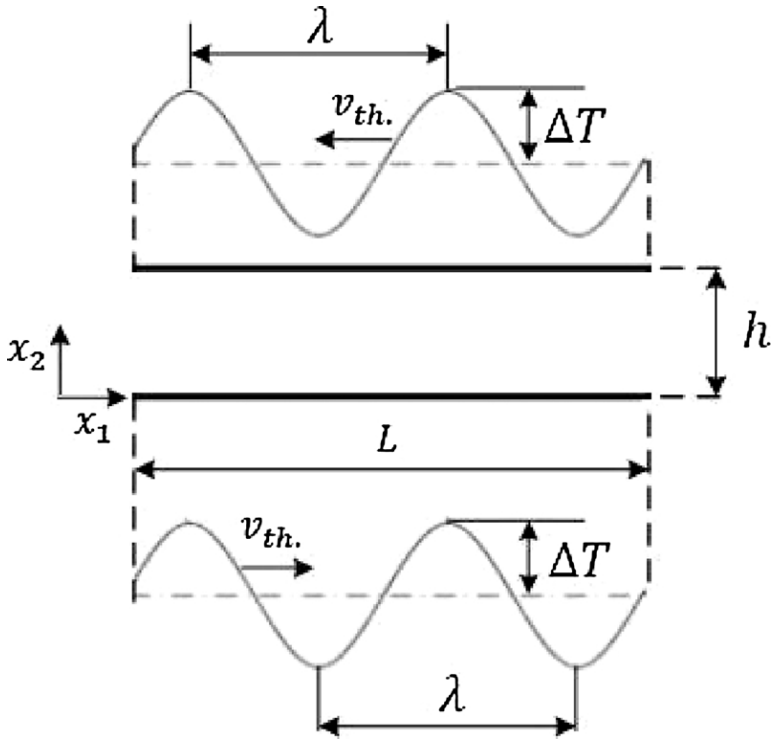

Figure 30: Problem geometry with boundary conditions

2.2 CAD Model and meshing of computational domain.

2D domain was constructed in ANSYS Design modeler. As discussed earlier, 2D domain was selected for ease of simulation. Figure 31 shows the mesh of computational domain. The height of the domain was 10 micrometers, while length is 200 micrometers.

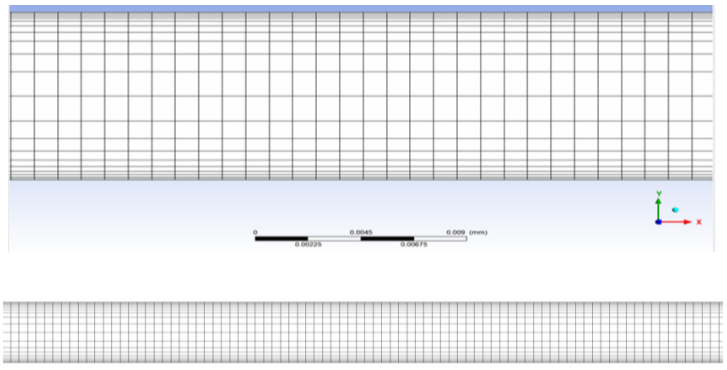

Figure 31: Mesh of computational domain

2.3 Boundary conditions

Figure 32 explains the boundary conditions of the computational domain. The entire domain was assumed symmetric. Inlet and outlet boundaries were specified as open boundary conditions. While upper and lower walls of the domain were assigned a time varying sinusoidal temperature profile moving in opposite direction. Time scale is kept as by the v=f λ as the reciprocal of frequency of the thermal waves as (λ/v_{th}) and time step in order of 0.01 times of the time scale. Fluid which is passed through the 2D pipe is simple water at reference temperature of 30℃. General thermal properties of water are following.

Table:1 Thermal properties of water at reference temperature at 30℃

Constraint	value
Thermal viscosity coefficient (η_T)	0.0215 K^{-1}
Density (ρ_0)	999.59 kg/m^3
Viscosity (μ_0)	8.79×10^{-4} Pa. s
Volumetric thermal expansion coefficient (α_T)	2.99×10^{-4} K^{-1}

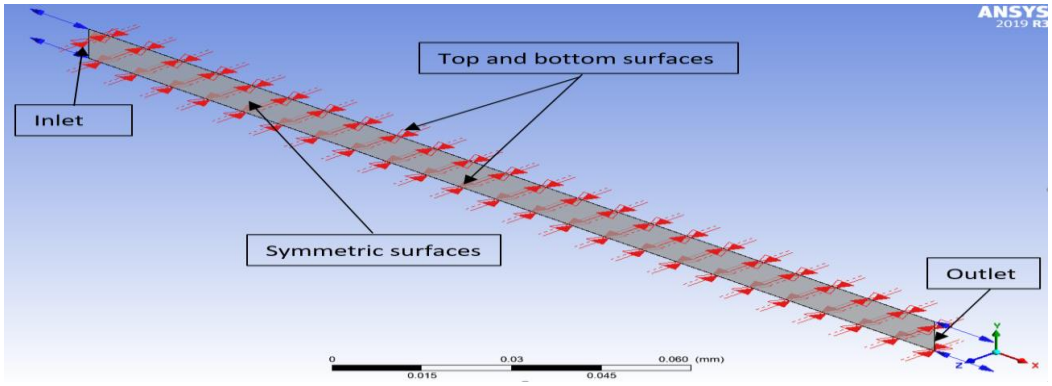

Figure 32: Boundary conditions of the computational domain

2.4 Solver and output controls

The laminar flow conditions were assumed. Thus, no turbulence was assumed to be produced. The convergence criteria were assumed to be 10^{-5}. Transient simulations were performed. The time step size of the simulation was λ dependent and described earlier.

CHAPTER 3: COMPUTATIONAL FLUID DYNAMICS IN ENGINEERIGN SIMULATIONS

Computational fluid dynamics (CFD) arose during WW II when engineers and scientists at the Los Alamos National Laboratory developed digital tools to describe the powerful fluxes produced by these devices, as well as atomic bombs. One of them was the mathematician von Neumann (J. von Neumann), who introduced the main synthetic viscosity method (Richmer and Morton, 1967) used to capture the effects of numerical solutions and is considered the father of CFD. His method immediately challenges the world's first programmable electronic computer. For the past 65 years, CFD is proud of this, along with its recognized theoretical and experimental fluid mechanics fields.

CFD technology creates a virtual reality that allows users of any size to fill all their traffic. This can be a droplet of particles passing through the micro channels of a small electromechanical system (MEMS), or it can be an air stream that raises the overall level. It can be a flame moving through the combustion chamber, or it can be the unstable melting core of a NPP. It could be the violent ocean and atmosphere on Earth, or it could be the gas disk of a spiral galaxy. Also, the concept of "overflow" is broad. Traffic flows along a multi-lane highway and towers move in phase space. Both can be handled using a contract for difference (CFD). Conclusionary the CFD method allows users to conduct virtual experiments. It can be "expensive, difficult, dangerous, or impossible" in the real world, according to P.L. low.

In most cases, a fluid can be viewed as a continuum that is described by the law of conservation and is expressed in the form of a partial differential equation (PDE), or as a continuum formulated for a small but finite volume fluid when using the integral equation. In CFD, these modeling equations are distributed over an arithmetic grid to produce finite fluctuations, finite magnitudes, or finite element approximations. If the fluid does not have enough collisions on the space-time scale in question, the fluid is no longer considered a continuum. Then, usually pseudo-particles are introduced, moving in the background grid and transferring/changing properties of the fluid. In aeronautical engineering, this method is used to describe the airflow around vehicles returning to the atmosphere, especially at high altitudes (see "Rare Gas Flow Calculation Models"). The CFD method is generally applied outside the range of flow parameters and experimental time and space scales, but the reliability of the calculated flow rate can only be

assessed under conditions of similar experimental and/or theoretical results. Standard practices are the most intolerable. Perform the same mathematical operations on grid sequences with higher precision. This "convergence study" gives you an idea of how close an accurate solution is to a PDE simulating flow physics. However, simulation errors still exist, and the experiments used for comparison have their own errors in setup and measurement conditions.

Due to the great interest in the modeling process, the demand and demand for computing solutions and methods of measuring and predicting the reliability of computing methods continues to grow. Therefore, it is currently booming in the fields of validation and verification (V&V) and uncertainty estimation (UQ) ("Verification and validation of CFD-based perturbation tests").

3.1 PRINCIPLES OF CFD

Since CFD involves numerical approximation of partial differential equations, a reliable set of numerical analysis principles must be followed.

3.1.1 Discretization

Computers can only store and process a limited amount of information. Therefore, the PDE decision should be presented with limited data. To do this, we usually use a mathematical network or network to divide the temporal and spatial continuum into small areas (networks or cells). The data can be described as a sample of points from a network node, suitable for finite difference method (FDM), or as an average value within the network, suitable for finite volume method (FVM).). In such cases, interpolation should be used to evaluate the detailed behavior of the solution within the network. Conversely, in finite element method (FEM), solutions within the network are detailed as the sum of the underlying functions, and the weights of these basic functions are independent data. The process of representing a solution with a simple set of data is called sampling, just like an approximation of a PDE that uses that data.

3.1.2 Consistency

The numerical approximation of the PDE must be consistent. When the grid cell size is set to infinite, the highlight disappears. To understand this, we assume that the shape of the PDE is ex (U) 0 and the finite difference is roughly FD (u) 0. Where u is the discrete point from the network

(j6x, n6t) to the node. Accurate PDE Equation solution u. We can treat these discrete values as point samples obtained from the exact solution of the slightly different PDE ex (u), TE (u). This is called the correction equation, and on the right is the truncation error, which is named because it is mainly caused by cutting the exact sequence of solutions around the node points.

3.1.3 Stability

If the interference of the solution is small at any point in the future, then the PDE's initial value problem is well suited. When applied to such a problem, the finite difference method is called the static method if a slight perturbation of the initial value causes a slight perturbation of the numerical solution later, regardless of the pixel size. For a stable flow problem, this "latency" becomes infinite, requiring a greater amount of absolute stability.

3.1.4 Convergence

When calculating discrete solution sequences in networks with increasing spatial and temporal resolution using the single difference method, you need to ensure that the sequences converge with the correct solution to the problem. In 1953, Lax demonstrated the famous theory of equivalence (Richtmyer and Morton, 1967), which was valid for linear approximation of a class of linear partial differential equations. This indicates that a combination of consistency and stability of the fluctuation plot is required and sufficient for convergence of numerical solutions.

3.1.5 Monotonicity

Starting with a monotonous distribution of initial values, a PDE like the heat load equation always produces a monotonous solution. Sampling and PDE are expected to share this characteristic. This type of chart is called monotonic or non-vibrating. It is clear that the monotone preservation system guarantees the positivity of the numerical solution based on positive data.

3.1.6 Conservation

The hydrodynamic equation describes the conservation of mass, momentum, and energy. In the case of discrete approximations, it is especially important to express the same principle to obtain an accurate shock wave propagation velocity.

CHAPTER 4: VALIDATION STUDY OF CFD MODEL

Meghdadi isfahani et al [12] published their work in journal of chemical engineering & process control, where established a mathematical model for the process behavior of 2D micro channels. The work focuses on keeping the wavelength constant at 100 micrometers. Their study was taken up as case mathematical model validation case.

4.1 Validation Case

The authors used the effects of viscous thermal expansion to create flow chaos and create suitable conditions for mixing the two liquids passing through the microchannel. They study 2D microchannels and use numerical simulations to quantify the disruption and focus on vortex changes to find the most effective flow parameters. They found that when a fluid flow is imposed on the microchannel by a pressure difference and two heat waves propagate in opposite directions, the fluid experiences a complex semi-static flow state. In some cases, this flow pattern develops into the corresponding chaotic convection. Using vortex as a control parameter indicating the amount of impairment, they showed that their method was suitable for mixing predicting oscillating flow in micro channels.

4.2 Comparison with simulated results

The comparison between the published results and simulated results is in figures (33, 34, 35 & 36). Comparison of figure 33 with published curves suggest that y directional velocity predicted by simulated results is validated. These figures are plotted by keeping λ = 100 micrometer, height h = 8 micrometer, ΔT =20℃ and v_{th}= 0.1 m/sec. The comparison indicates that the maximum velocity in the channel is 175 µm/sec. This is in agreement with the published data.

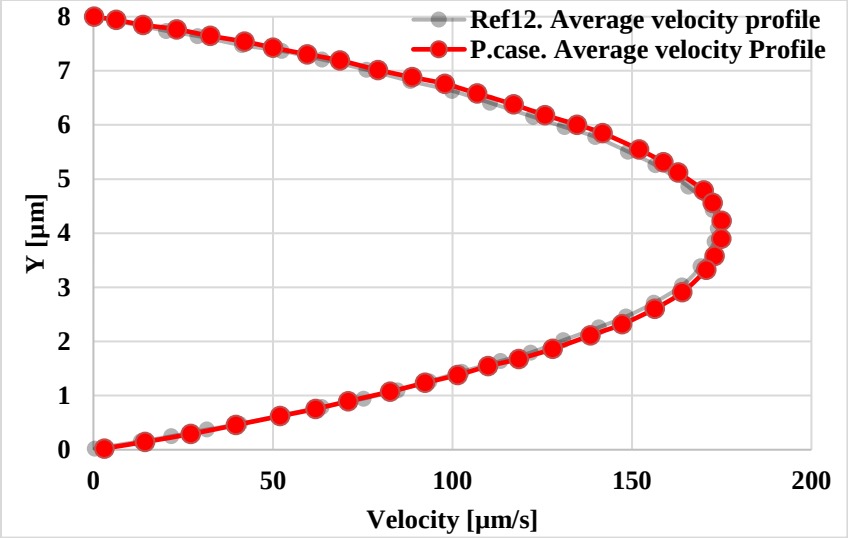

Figure 33: Comparison of Velocity distribution between published case and simulated case

Figure 34 depicts the time average dimensionless vorticity plots versus dimensionless velocity for various values of h /δth. Comparing the two results it can be seen that the simulated results are very well in agreement with the published results as in both figures chaotic mixing is achieving almost about 0.54 value of horizontal axis of U_{th}/U. Same is true for figures 35 the plots between the ratio of characteristic velocities of thermal waves and the normalized standard deviation (NSD) of the nondimensional mean vorticity which is also considered as the extension of last validated vorticity curve.

The last validation of the work is relation between Reynold number and Strouhal number for various values of U_{th}/U. From fig. 36 we can see that all the trend and each value of our simulated work absolute same as published work.

From the comparison of all the figures it can be seen that developed model is accurate as the results predicted by it matches with the results of the simulated results. Hence the model can be further examined to predict the behavior of the microchannel for various parameters.

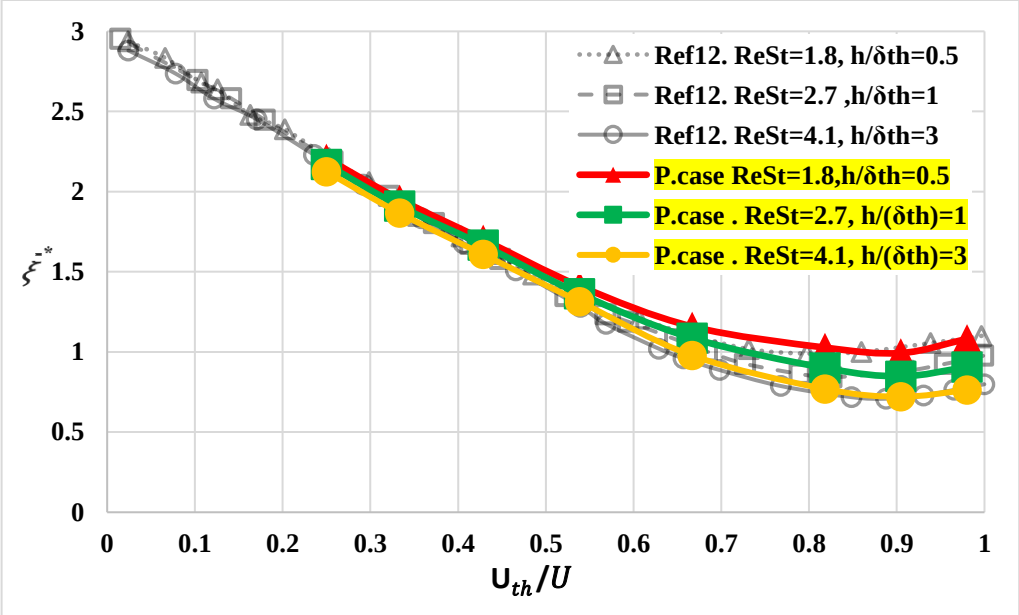

Figure 34: Comparison of Time averaged dimensionless mean vorticity vs U_{th}/U for h/δ_{th} (3,1,0.5) between validated case and simulated case

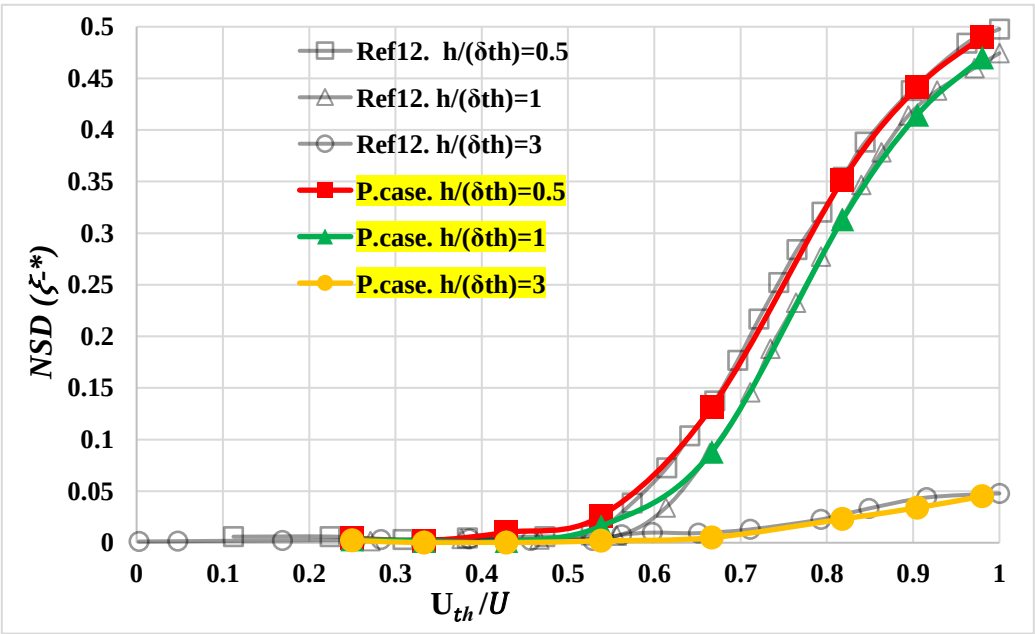

Figure 35:

Comparison of Variation of NSD with dimensionless velocity between validated case and simulated case

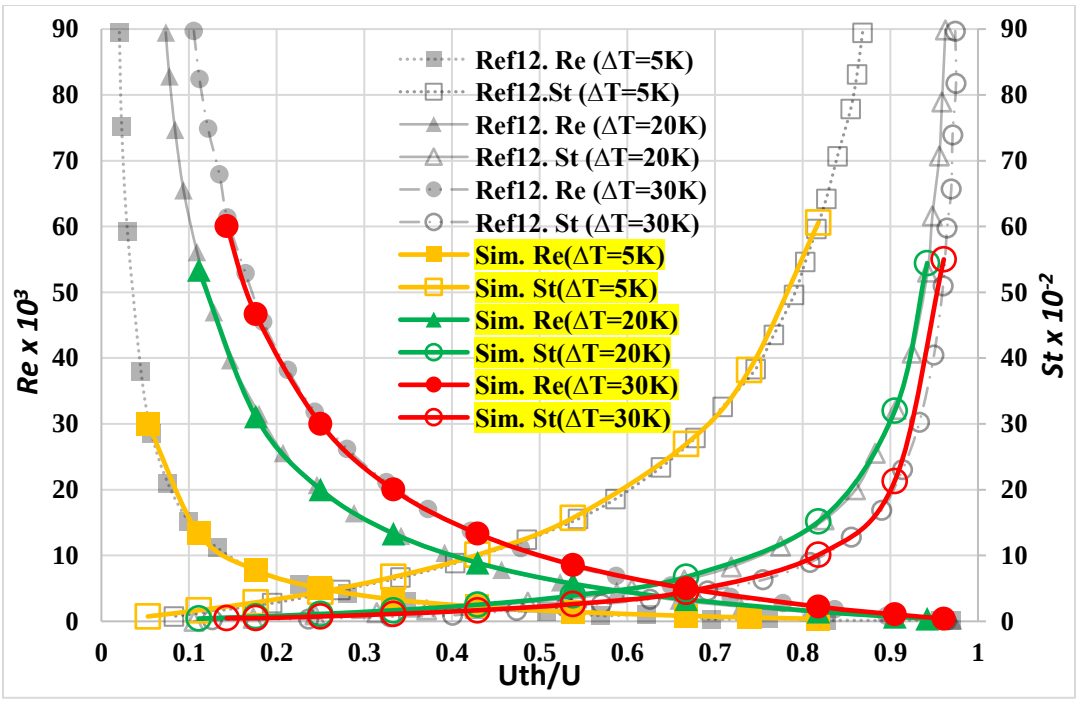

Figure 36: Comparison of variation of Re and St verses U_{th}/U for different values of ΔT, h=10 µm, λ =100 µm and v_{th} =0.1 m/sec between validated case and simulated case for simulated case

CHAPTER 5: RESULTS AND DISCUSSIONS

As discussed in the previous chapter the mathematical model thus established is validated for the wavelength λ = 100 µm, h=10 µm, v_{th} =0.1 m/sec. The model was thus further extrapolated to predict the behavior of the micro system for various wavelength values like 100µm, 150µm, 200µm and 50µm. The length of simulated channel was kept at 200 micrometers. The results and discussion of the simulated results are as follows.

5.1 CASE: A λ=100µm

Figures 37 to 43 show the variation of various parameters with the wavelength of 100 micrometer. Fig. 37 is plotted between the nondimensional average vorticity and characteristic velocities ratio of thermal waves and total characteristic velocity for different values of h/ δth. Horizontal axis values of U_{th}/U is zero to unity. Minimum value of zero of U_{th}/U corresponds to Poiseuille flow and maximum value of it shows that thermal waves as a dominant parameter towards the fluid mixing. The variation of U_{th}/U from zero to 1 demonstrate the shared flow due to thermal waves and differential pressure. From fig. 37 it is concluded that when the value of U_{th}/U is decreased up to zero then all the graphs meet at vertical axis of nondimensional vorticity ($\widetilde{\xi^*}$) approximate to 3 saying Poiseuille flow lonely flow persuader. So, by moving from left to right we can see that all plots tend to disperse from each other at $U_{th}/U \geq 0.54$ showing that mixing due to the thermal waves (TVEC) effect is achieved at 0.54. This is the value ($0.54 \leq U_{th}/U \leq 1$) upon which flow is due to combined effect of differential pressure and TVEC effect and this mixing can be improved by reducing the value of h/ δth as vorticity is considered as criteria for describing the mixing mechanisms of engulfment, stretching and species gradient change. For determining these non-dimensional number (U_{th}/U, h/ δth) we assumed the work due to pressure and viscid dissipation is approximately zero as this is supposition where efficiency due to thermal waves is higher because major role in mixing is of TVEC effect.

According to figure 37 as the velocity ratio is increased mean vorticity is decreased. It can be seen from the figure that the maximum value of 2.25 exits for ReSt value of 1.8 and minimum at 2.15 for ReSt of 4.1, close to region where the Poiseuille flow is dominant. These values change to 1.1, 0.8 and 0.7 for area dominant by thermal wave induced mixing at ReSt value of 1.8, 2.7 and 4.1,

respectively. Differential pressure Δp is reduced from 80.26 Pa to 35.18 Pa with reduction of h/δ_{th} corresponding values (3,1,0.5) resulting increase in thermal penetration length(δ_{th}) 3.33, 10 and 20μm.

Table 2: Variation of Vorticity and NSD of vorticity for λ=100μm

λ (μm)	h/δ_{th}	$U_{th}U$	U_{th}/U	Δp	ReSt	Vorticity ($\bar{\xi}^*$)	NSD ($\bar{\xi}^*$)
100	0.496	0.400	0.250	60.895	1.80	2.158	0.004
100	0.496	0.500	0.333	40.597	1.80	1.939	0.002
100	0.496	0.600	0.429	27.064	1.80	1.702	0.010
100	0.496	0.700	0.538	17.399	1.80	1.451	0.026
100	0.496	0.800	0.667	10.149	1.80	1.209	0.131
100	0.496	0.900	0.818	4.511	1.80	1.027	0.351
100	0.496	0.950	0.905	2.137	1.80	0.993	0.441
100	0.496	0.990	0.980	0.410	1.80	1.018	0.490
100	1.001	0.400	0.250	91.533	2.70	2.120	0.003
100	1.001	0.500	0.333	61.022	2.70	1.899	0.002
100	1.001	0.600	0.429	40.681	2.70	1.656	0.002
100	1.001	0.700	0.538	26.152	2.70	1.393	0.018
100	1.001	0.800	0.667	15.255	2.70	1.126	0.101
100	1.001	0.900	0.818	6.780	2.70	0.905	0.313
100	1.001	0.950	0.905	3.212	2.70	0.848	0.415
100	1.001	0.990	0.980	0.616	2.70	0.855	0.470
100	3.00	0.40	0.25	138.92	4.10	2.06	0.002
100	3.00	0.50	0.33	92.61	4.10	1.85	0.000
100	3.00	0.60	0.43	61.74	4.10	1.60	0.000
100	3.00	0.70	0.54	39.69	4.10	1.33	0.000
100	3.00	0.80	0.67	23.15	4.10	1.05	0.001
100	3.00	0.90	0.82	10.29	4.10	0.80	0.010
100	3.00	0.95	0.90	4.87	4.10	0.72	0.019
100	3.00	0.99	0.98	0.94	4.10	0.71	0.050

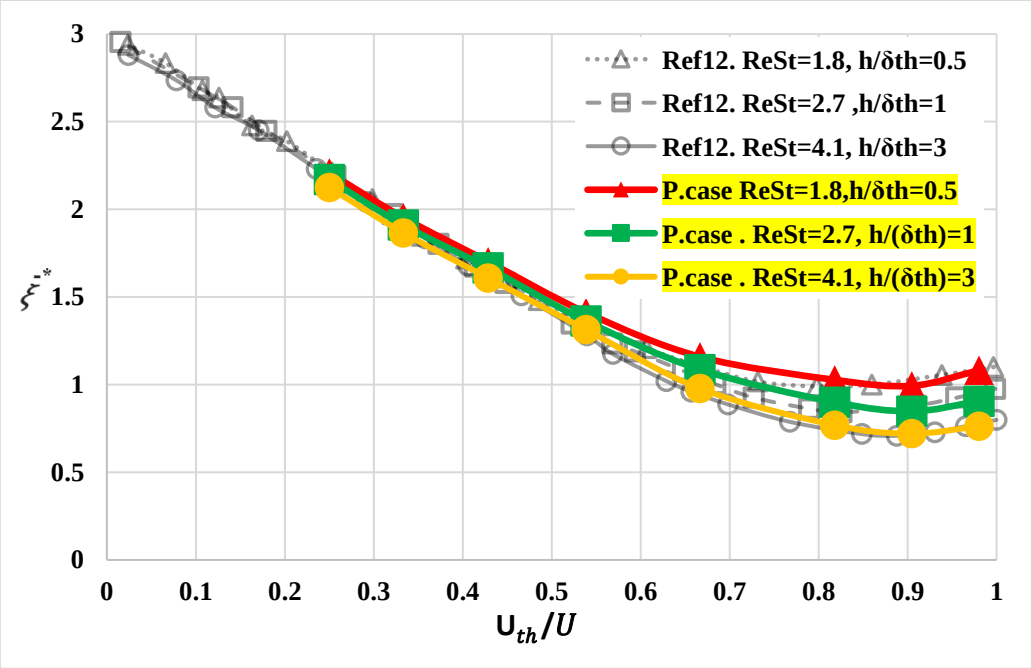

Figure 37: Nondimensional mean vorticity verses U_{th}/U for λ=100μm compared to published case

Normalized Standard Deviation (NSD) plots of vorticity are given in Figure 38. For the 2D system of chaotic mixing it is an important feature to change the variables regularly with in the physical confines. NSD is used as this variation calculated by

$$\text{NSD (x(a))} = \frac{1}{\bar{x}}\sqrt{\int [x(a) - \bar{x}]\text{^}2 \ * da} \ , \ \bar{x} = \frac{1}{a-a0}\int_{a0}^{a} x(a)da$$

Where x is used as the rise of change in the parameters within the bounds. Fig. 38 is plotted between the intensification of vorticity and U_{th}/U. It can be concluded from this plot is that vorticity value is approximately negligible at small values of U_{th}/U and this rises at specific value of velocity ratio like ≥0.54 with different slopes which are related directly to the values of h/ δth . At small values of U_{th}/U vorticity change is negligible showing that in this region differential pressure is higher near Poiseuille flow region so flow is steady and facing very minor oscillation in velocity arenas. So, by reducing this Δp these oscillations become more competent due to TVEC effect causing flow in semi steady state and finally resulting in chaotic flow.

For wavelength 100 micrometer values of h/ δth varies from 0.5 to 3.0. As the dimensionless velocity increases these values also increase reaching a top NSD of vorticity of 0.075, 0.47 and

0.49 for h/ δth values of 3, 1, 0.5, respectively. Increasing thermal penetration length into the fluid may result in increase in variation intensification NSD of dimensionless mean vorticity.

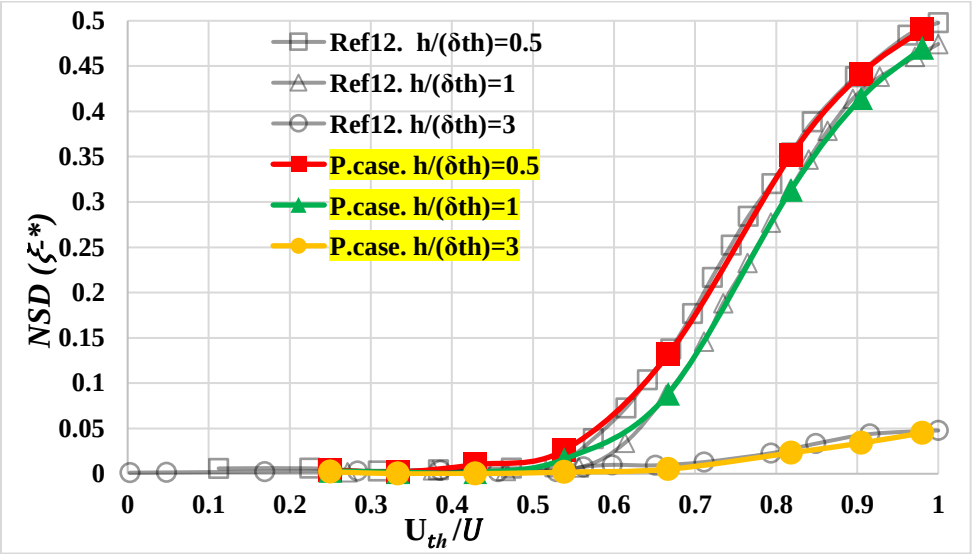

Figure 38: NSD of vorticity for λ=100μm compared to published case

Fig 39 clarifies the effect of U_{th}/U on Reynold number and Strouhal number at various values of temperature wave amplitudes. We can determine the extreme bound of Reynold number in which flow is made chaos and chaotic mixing is completed. But this limit is strongly dependent on the ΔT and velocity ratio. We can use this plot after achieving results of fig. 37 & 38 like we have come to known that chaotic mixing achieving and increasing at values of ≥0.54 of U_{th}/U, so we can find maximum Re number bound for any selected value of ΔT.

We can conclude from this figure that increase in the value of U_{th}/U causing drop in Reynold number with drop in differential pressure, but Strouhal number experiences an elevation which is suitable for chaotic mixing increments.

Mixing due to TVEC effect is achieved at U_{th}/U value ≥0.54 so at this value fig 39 shows that maximum probable bound of Re is 8.58×10^{-3} for ΔT of 30K. Same can be determined for ΔT 20K which is 5.72×10^{-3} and 1.43×10^{-3} for ΔT 5K. With drop in Re number St number rises to 2.62×10^{-2} for 30K, $3.92\times 10^{-2}$for 20K and 15.72×10^{-2} for 5K amplitudes. As the Re number is falling with same ratio St number is increasing contributing towards the chaos flow due to TVEC effect.

Table 3: Variation of Re and St for λ=100 μm

ΔT	$U_{th}U$	U_{th}/U	ΔP	Re*1000	St /100	2*St /100
20K	0.97	0.942	0.4	0.413	27.22	54.44
	0.95	0.905	0.7	0.702	15.99	31.98
	0.9	0.818	1.4	1.483	7.58	15.16
	0.8	0.667	3.2	3.336	3.37	6.74
	0.7	0.538	5.4	5.718	1.96	3.92
	0.6	0.429	8.5	8.895	1.26	2.52
	0.5	0.333	12.7	13.343	0.84	1.68
	0.4	0.25	19	20.015	0.56	1.12
	0.3	0.176	29.6	31.134	0.36	0.72
	0.2	0.111	50.7	53.373	0.21	0.42
30K	0.98	0.961	0.4	0.408	27.5	55
	0.95	0.905	1	1.053	10.66	21.32
	0.9	0.818	2.1	2.224	5.05	10.1
	0.8	0.667	4.8	5.004	2.24	4.48
	0.7	0.538	8.2	8.578	1.31	2.62
	0.6	0.429	12.7	13.343	0.84	1.68
	0.5	0.333	19	20.015	0.56	1.12
	0.4	0.25	28.5	30.022	0.37	0.74
	0.3	0.176	44.4	46.701	0.24	0.48
	0.25	0.143	57.1	60.044	0.19	0.48
5K	0.9	0.818	0.4	0.371	30.3	60.6
	0.85	0.739	0.6	0.589	19.08	38.16
	0.8	0.667	0.8	0.834	13.47	26.94
	0.7	0.538	1.4	1.43	7.86	15.72
	0.6	0.429	2.1	2.224	5.05	10.1
	0.5	0.333	3.2	3.336	3.37	6.74
	0.4	0.25	4.8	5.004	2.24	4.48
	0.3	0.176	7.4	7.784	1.44	2.88
	0.2	0.111	12.7	13.343	0.84	1.68
	0.1	0.053	28.5	30.022	0.37	0.74

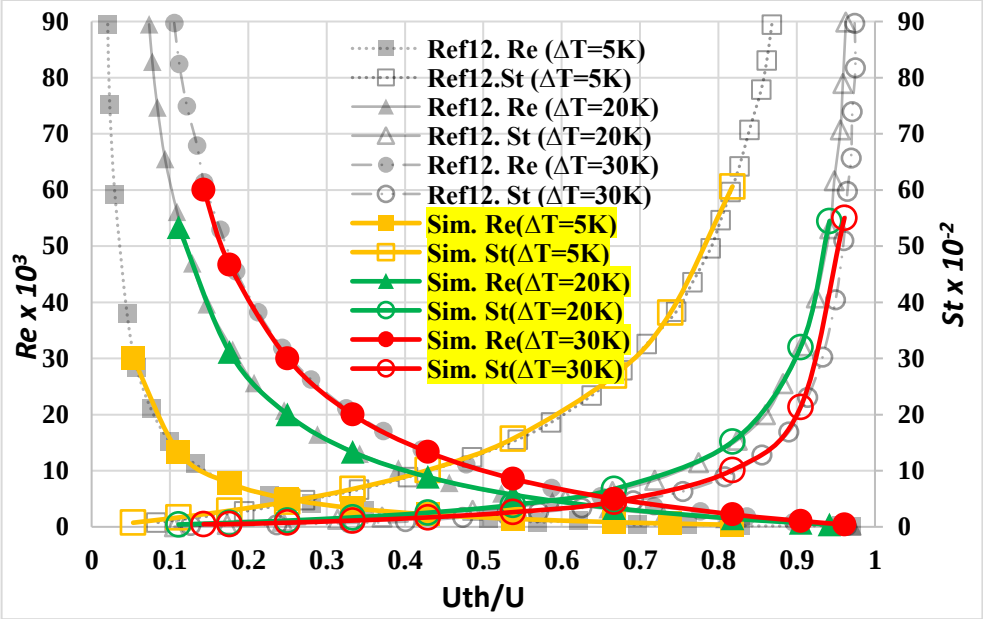

Figure 39: Variation of Re & St for λ=100µm compared to published case

Contours of Normalized total pressure, Normalized temperature, Normalized velocity u and Normalized vorticity at 100th time step is plotted for wavelength 100 micrometer from figure 40 to 43.

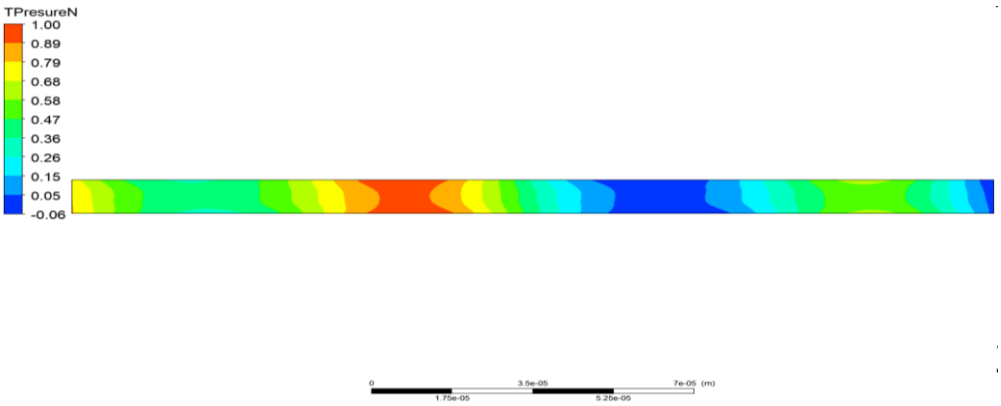

Figure 40: Normalized Pressure Variation for 100 µm

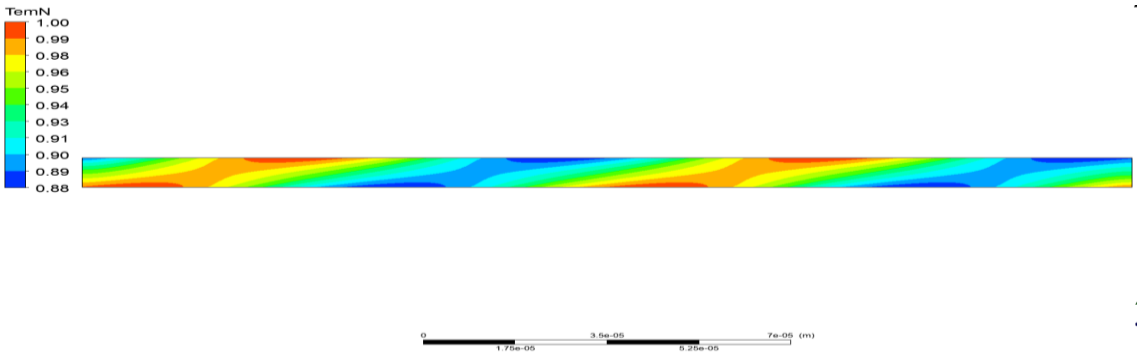

Figure 41: Normalized Temperature Variation for 100 µm

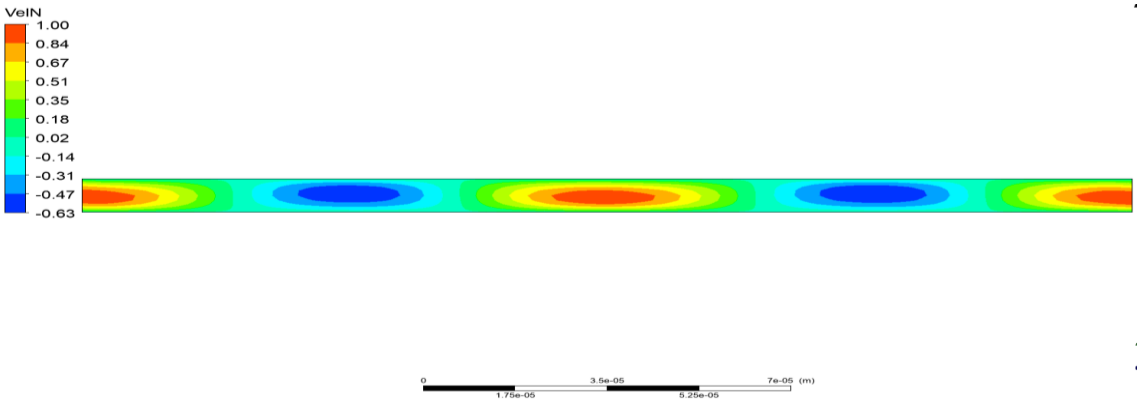

Figure 42: Normalized Velocity Variation for 100 µm

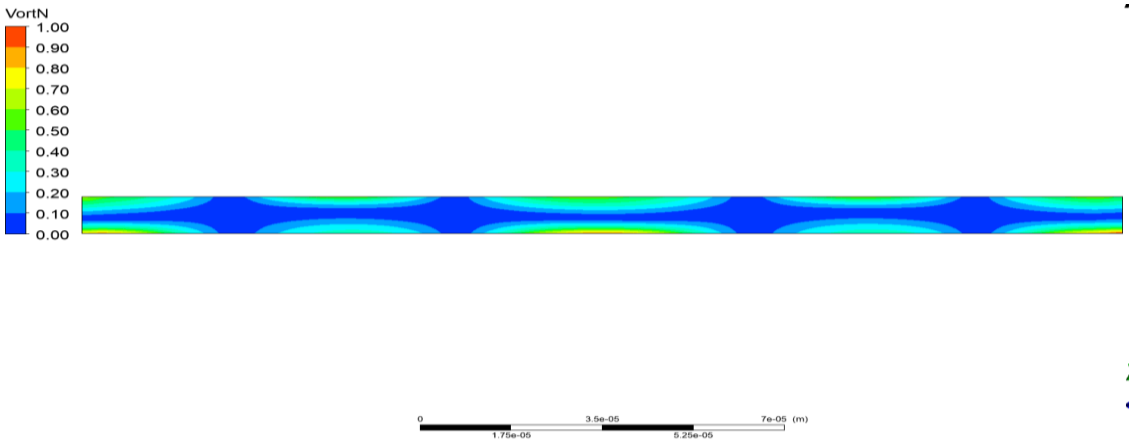

Figure 43: Normalized Vorticity Variation for 100 µm

5.2 CASE: B λ=150μm

Figures 44 shows the comparison of simulation case with validated case by varying of various parameters at 150μm wavelength. The change in mean vortex is shown in Figure 44. From equation (8) we see that thermal diffusion length δ_{th} is directly proportional to the square root of wavelength λ . So, when the wavelength is increased from 100 to 150 micrometer so δ_{th} increases quadratically. Thermal diffusion increment also causes to increase in mixing time to reside the thermal waves in fluid for more time resulting in more mixing. So, we can see that the average vorticity curves decrease as the speed increases. By comparing with published case, all graphs now tend to separate from each other at $U_{th}/U \geq 0.64$ approximately increasing the thermal mixing efficiency from 0.54 to 0.64. So, it is very beneficial towards making the flow chaos. From fig.44 is also very clear that nondimensional number $\frac{h}{\delta_{th}}$ is experiencing a drop for different values of ReSt because denominator δ_{th} is rising with wavelength λ .So with further decrease in $\frac{h}{\delta_{th}}$ results in increase in vorticity. As can be seen from the figure, the maximum value of vorticity for Poiseuille flow 3.09 corresponds to the ReSt value of 1.8, and the minimum value of 3.04 corresponds to the ReSt value of 4.1, indicating that the Poiseuille flow is close to the dominant area. For regions where heat wave mixing is dominant, these $\frac{h}{\delta_{th}}$ values have changed from 3, 1, and 0.5 to 2.45, 0.82 and 0.41 respectively because thermal penetration length is increased from 3.33 to 4.08μm, 10 to 12.16μm and 20 to 24.39μm with respective drop of $\frac{h}{\delta_{th}}$ values. So, by comparing with case A mixing due to TVEC effect is increased from 0.79, 0.97 and 1.1 to 0.87,1.04 and 1.23 for the corresponding values of h/ δ_{th} of 2.45,0.82 and 0.41 and ReSt values.

Table 4: Variation of Vorticity and NSD vorticity for λ=150μm

λ (μm)	h/δ_{th}	$U_{th}U$	U_{th}/U	ΔP	ReSt	Vorticity $\bar{\xi}^*$	NSD($\bar{\xi}^*$)
150	0.405	0.400	0.333	60.895	1.80	3.097	0.004
150	0.405	0.500	0.429	40.597	1.80	2.687	0.006
150	0.405	0.600	0.529	27.064	1.80	2.271	0.018
150	0.405	0.700	0.636	17.399	1.80	1.861	0.048
150	0.405	0.800	0.750	10.149	1.80	1.489	0.160
150	0.405	0.900	0.871	4.511	1.80	1.213	0.320
150	0.405	0.950	0.934	2.137	1.80	1.146	0.441
150	0.405	0.990	0.987	0.410	1.80	1.148	0.550

150	0.817	0.400	0.333	91.533	2.70	3.049	0.003
150	0.817	0.500	0.429	61.022	2.70	2.636	0.005
150	0.817	0.600	0.529	40.681	2.70	2.212	0.005
150	0.817	0.700	0.636	26.152	2.70	1.787	0.032
150	0.817	0.800	0.750	15.255	2.70	1.385	0.120
150	0.817	0.900	0.871	6.780	2.70	1.067	0.280
150	0.817	0.950	0.934	3.212	2.70	0.977	0.401
150	0.817	0.990	0.987	0.616	2.70	0.965	0.510
150	2.45	0.40	0.33	138.92	4.10	2.98	0.003
150	2.45	0.50	0.43	92.61	4.10	2.57	0.004
150	2.45	0.60	0.53	61.74	4.10	2.15	0.003
150	2.45	0.70	0.64	39.69	4.10	1.71	0.008
150	2.45	0.80	0.75	23.15	4.10	1.29	0.010
150	2.45	0.90	0.87	10.29	4.10	0.94	0.040
150	2.45	0.95	0.93	4.87	4.10	0.83	0.090
150	2.45	0.99	0.99	0.94	4.10	0.81	0.110

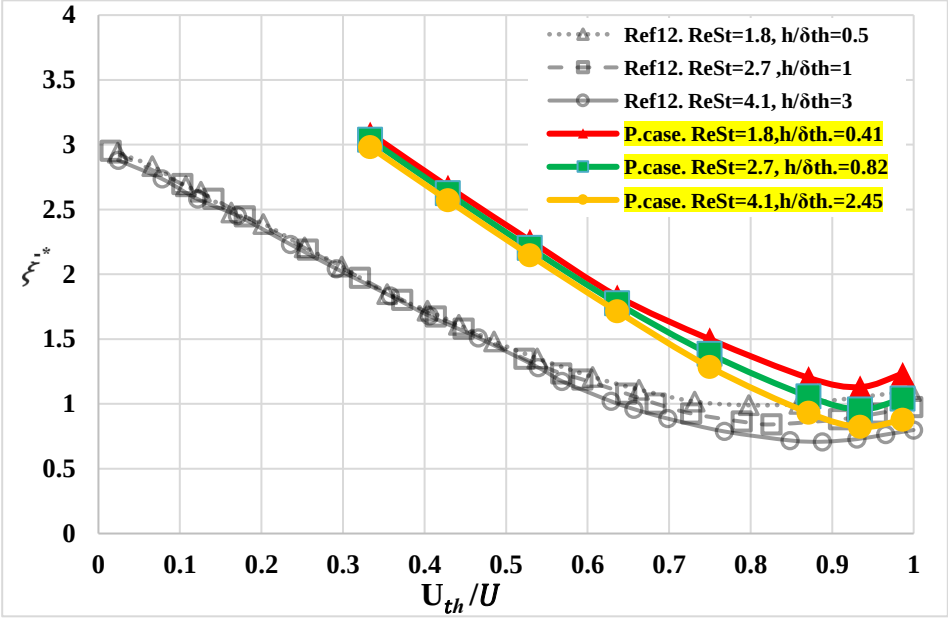

Figure 44: Dimensionless mean vorticity for λ=150 µm compared to validated case A

A graph of the normal standard deviation (NSD) of the vortex is shown in Figure 45. For 150 µm, the $\frac{h}{\delta th}$ value is in the range of 0.41 to 2.45. As the dimensionless velocity increases, these values also increase with very low value near to zero deviation from mean and rise to a value of approximately 0.64 with slope directly related to $\frac{h}{\delta th.}$ value. As this value faces drop NSD will

rise. By comparing the previous case of 100 μm this deviation is risen to 0.55for ratio 0.41 of $\frac{h}{\delta th}$. So NSD can be elevated by reducing this nondimensional number $\frac{h}{\delta th}$ values of 0. 41, 0.82 and 2.45 have the upper vortex NSDs are 0.55, 0.51 and 0.11, respectively.

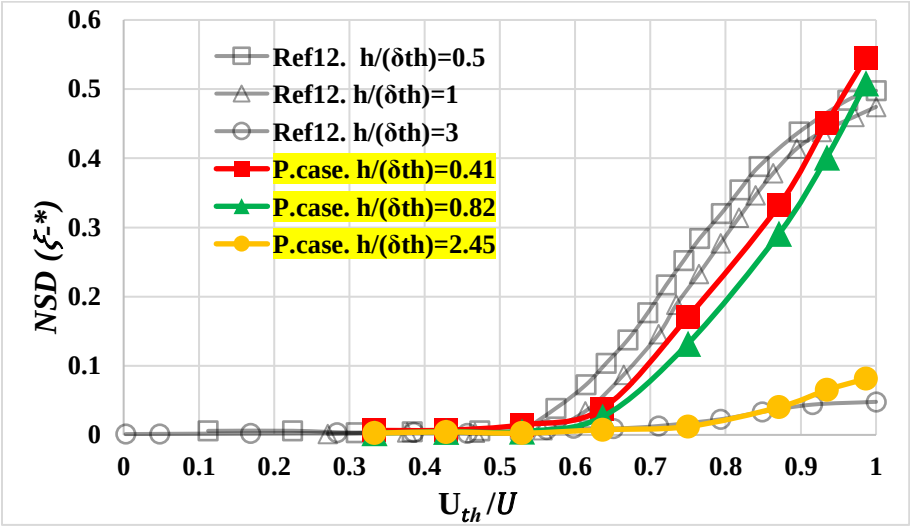

Figure 45: NSD of vorticity for λ=150μm compared to the validated case A

From the figures 44 & 45 it is found that chaotic fluid mixing is accomplished at $U_{th}/U \geq 0.64$ so from fig 46 it is easy to find out the extreme values region of Re number and St number. As the U_{th}/U volume speed increases, the Re number decreases and the Strouhal number increases. The figure shows that when mixing due to TVEC effect and differential pressure is attained ($U_{th}/U \geq 0.64$) than Re number for ΔT 30K drops up to 5.72×10^{-3} which was 8.58×10^{-3} in previous case. Re number further decreases to 3.8×10^{-3} and 0.95×10^{-3} for 20K and 5K ΔT, respectively. With the reduction of Re number St climbs up to 3.93×10^{-2} ,5.89×10^{-2} and 23.57×10^{-2} for 30K,20K and 5K amplitudes, respectively.

Table 5: Variation of Re and St for λ=150 μm

ΔT	$U_{th}U$	U_{th}/U	ΔP	Re*1000	St /100	2*St /100
20K	0.97	0.96	0.4	0.275	40.83	81.65
	0.95	0.934	0.7	0.468	23.99	47.98
	0.9	0.871	1.4	0.988	11.36	22.73
	0.8	0.75	3.2	2.224	5.05	10.1
	0.7	0.636	5.4	3.812	2.95	5.89
	0.6	0.529	8.5	5.93	1.89	3.79
	0.5	0.429	12.7	8.895	1.26	2.53
	0.4	0.333	19	13.343	0.84	1.68
	0.3	0.243	29.6	20.756	0.54	1.08
	0.2	0.158	50.7	35.582	0.32	0.63
30K	0.97	0.96	0.6	0.413	27.22	54.43
	0.95	0.934	1	0.702	15.99	31.99
	0.9	0.871	2.1	1.483	7.58	15.15
	0.8	0.75	4.8	3.336	3.37	6.73
	0.7	0.636	8.2	5.718	1.96	3.93
	0.6	0.529	12.7	8.895	1.26	2.53
	0.5	0.429	19	13.343	0.84	1.68
	0.4	0.333	28.5	20.015	0.56	1.12
	0.3	0.243	44.4	31.134	0.36	0.72
	0.2	0.158	76.1	53.373	0.21	0.42
5K	0.97	0.96	0.1	0.069	163.3	326.6
	0.95	0.934	0.2	0.117	95.96	191.92
	0.9	0.871	0.4	0.247	45.45	90.91
	0.8	0.75	0.8	0.556	20.2	40.4
	0.7	0.636	1.4	0.953	11.78	23.57
	0.6	0.529	2.1	1.483	7.58	15.15
	0.5	0.429	3.2	2.224	5.05	10.1
	0.4	0.333	4.8	3.336	3.37	6.73
	0.3	0.243	7.4	5.189	2.16	4.33
	0.2	0.158	12.7	8.895	1.26	2.53

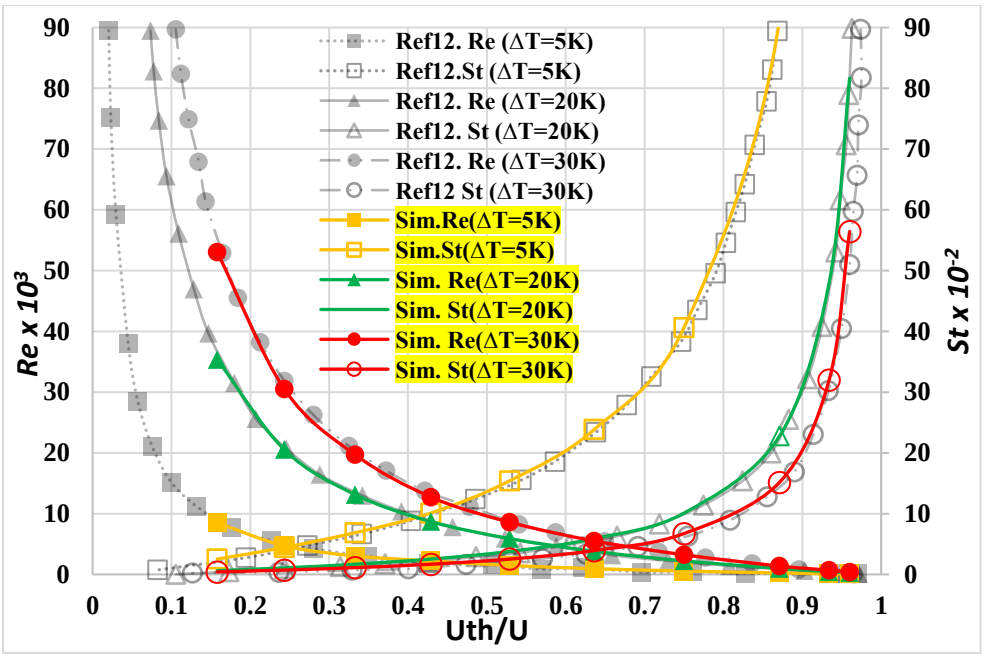

Figure 46: Variation of Re and St for λ=150µm compared to the published case A

For 150µm in Figures 47-50, the normal total pressure, normal temperature, normal velocity u, and the normal vortex line for the 100th time step are shown.

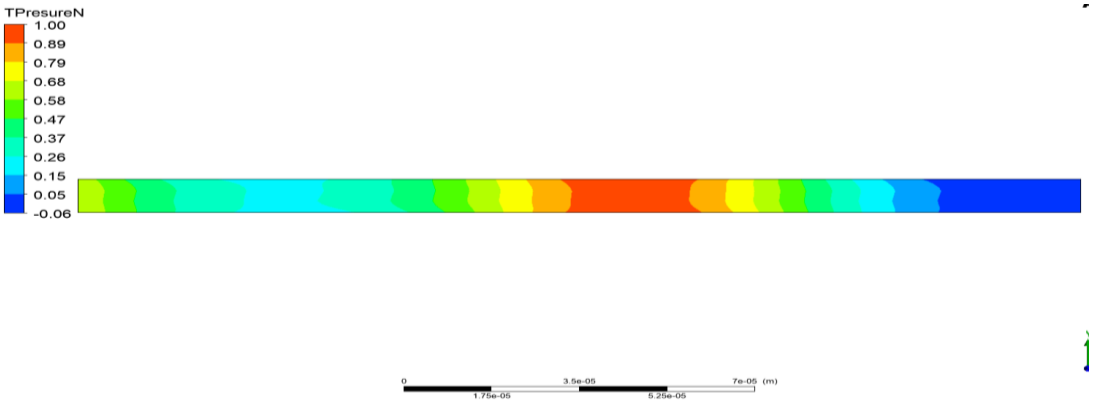

Figure 47: Normalized Pressure Variation for λ=150µm

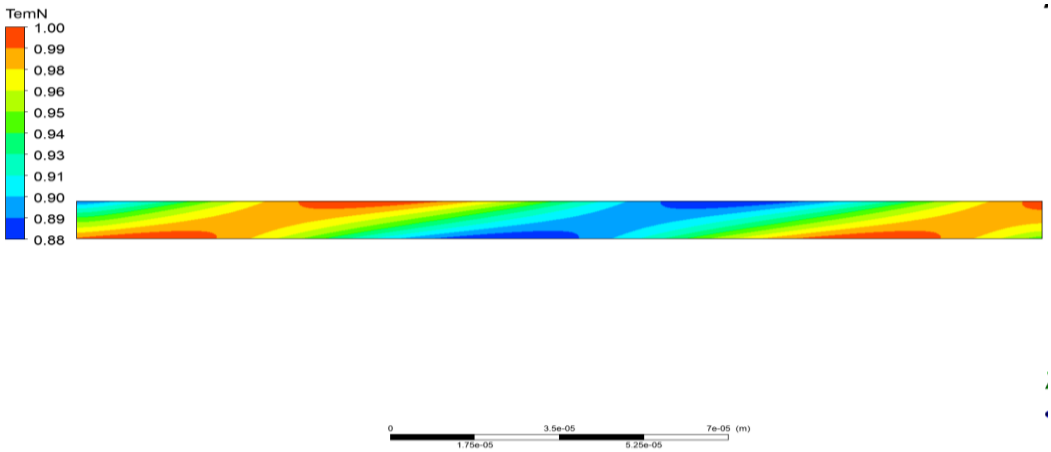

Figure 48: Normalized Temperature Variation for λ=150 µm

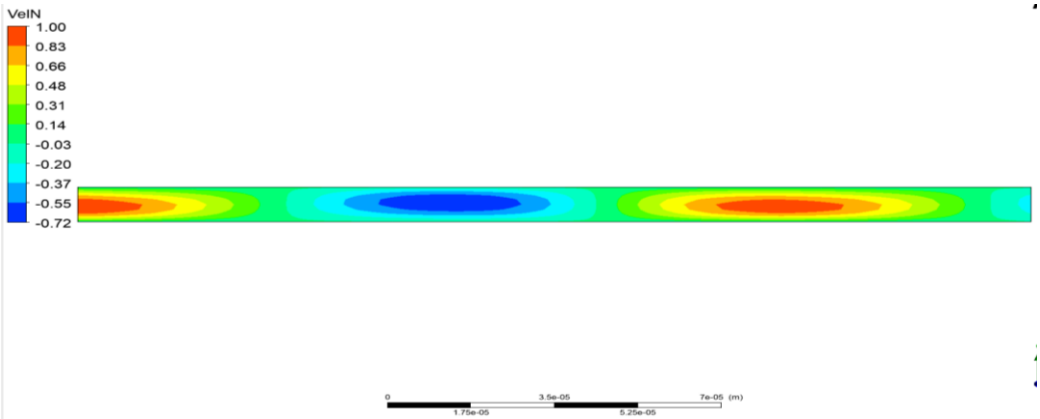

Figure 49: Normalized Velocity Variation for λ=150µm

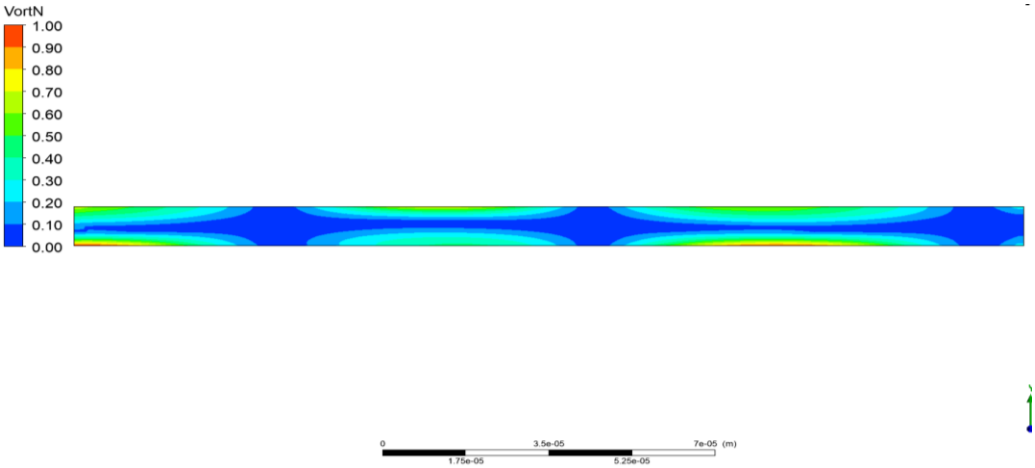

Figure 50: Normalized Vorticity Variation for λ=150µm

5.3 CASE: C λ=200μm

Figures 51-53 show the variation of various parameters at wavelength 200μm. The change in mean vortex is shown in Figure 51. We can see that the average vorticity decreases as the speed increases experiencing pressure drop. In the figure, a maximum value of 3.5 corresponds to a ReSt value of 1.8, and a minimum value of 3.48 corresponds to a ReSt value of 4.1, indicating that the Poiseuille flow is close to the dominant area. For regions where mixed heat waves dominate, these values changed 1.37, 1.16, and 0.97, respectively for ReSt values were 1.8, 2.7, and 4.1, respectively. Chaotic mixing due to TVEC effect is accomplished now at $U_{th}/U \geq 0.69$ approximately. So, mixing efficiency due to this effect is elevating ($U_{th}/U \geq 0.69$) with increment in wavelength as time for mixing is also directly related to wavelength. Nondimensional average vorticity is enhanced with reduction of $\frac{h}{\delta th.}$ which is reduced from 0.41 to 0.35 (ReSt=1.8), 0.82 to 0.71 (ReSt=2.7) and 2.45 to 2.12 (ReSt=4.1) as compared to previous published case of λ=100μm. Thermal penetration length increased to 3.33 to 4.72μm, 10 to 14.08 μm and 20 to 28.57 μm with corresponding values of h/ δ_{th} 2.12 ,0.71 and 0.35, respectively. So, by comparing with validated case chaotic mixing ($\bar{\xi}^*$ **)** due to TVEC effect is increased from 0.99 to 1.40 which is higher to case A values (0.77 to 1.1).

Table 6: Variation of Vorticity and NSD vorticity for λ=200μm

λ (μm)	h/δ_{th}	U_{th}U	U_{th}/U	ΔP	ReSt	Vorticity $\bar{\xi}^*$	NSD ($\bar{\xi}^*$)
200	0.351	0.400	0.400	60.895	1.80	3.527	0.010
200	0.351	0.500	0.500	40.597	1.80	2.994	0.020
200	0.351	0.600	0.600	27.064	1.80	2.490	0.025
200	0.351	0.700	0.700	17.399	1.80	2.034	0.070
200	0.351	0.800	0.800	10.149	1.80	1.658	0.401
200	0.351	0.900	0.900	4.511	1.80	1.413	0.750
200	0.351	0.950	0.950	2.137	1.80	1.362	0.950
200	0.351	0.990	0.990	0.410	1.80	1.370	1.020
200	0.708	0.400	0.400	91.533	2.70	3.486	0.008
200	0.708	0.500	0.500	61.022	2.70	2.945	0.010
200	0.708	0.600	0.600	40.681	2.70	2.425	0.010
200	0.708	0.700	0.700	26.152	2.70	1.943	0.040
200	0.708	0.800	0.800	15.255	2.70	1.529	0.300
200	0.708	0.900	0.900	6.780	2.70	1.238	0.650
200	0.708	0.950	0.950	3.212	2.70	1.166	0.850

200	0.708	0.990	0.990	0.616	2.70	1.160	0.930
200	2.12	0.40	0.40	138.92	4.10	3.43	0.002
200	2.12	0.50	0.50	92.61	4.10	2.89	0.003
200	2.12	0.60	0.60	61.74	4.10	2.36	0.005
200	2.12	0.70	0.70	39.69	4.10	1.86	0.010
200	2.12	0.80	0.80	23.15	4.10	1.41	0.050
200	2.12	0.90	0.90	10.29	4.10	1.07	0.080
200	2.12	0.95	0.95	4.87	4.10	0.98	0.110
200	2.12	0.99	0.99	0.94	4.10	0.96	0.150

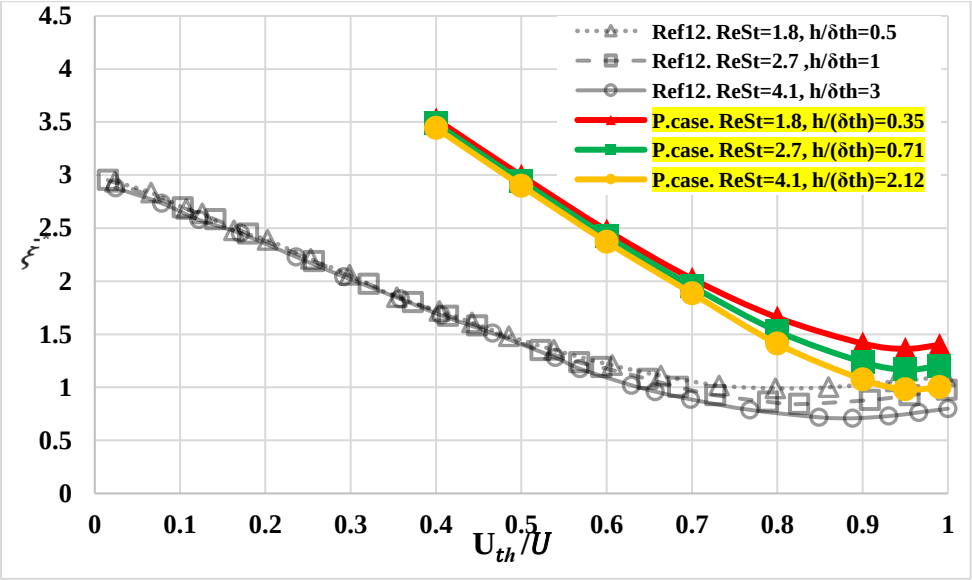

Figure 51: Dimensionless mean vorticity for λ=200μm compared to published case A

A plot of the standard deviation (NSD) is shown in Figure 52. For 200μm, we can see that the $\frac{h}{\delta th.}$ is between 0.35 and 2.12. As the dimensionless velocity increases, NSD of ($\bar{\xi}^*$) also increase slowly up to almost $U_{th}/U \geq 0.69$ and then rise sharply depending on the $\frac{h}{\delta th.}$ value. This deviation rises as the value of $\frac{h}{\delta th.}$ reduces. As compared the previous cases and published case NSD of vorticity is higher as because of reduction of nondimensional number h/ δth reaching the highest NSD vortices 0.642, 0.61 and 0.115 with values of h/δth 0.35, 0.71 and 2.12, respectively. So, for larger values of Δp fluid flow steadily and experiences small actuations in velocity field so when

thermal effect is dominated due to small values of pressure fluid face higher whirling complex structures which contributes towards mixing increments.

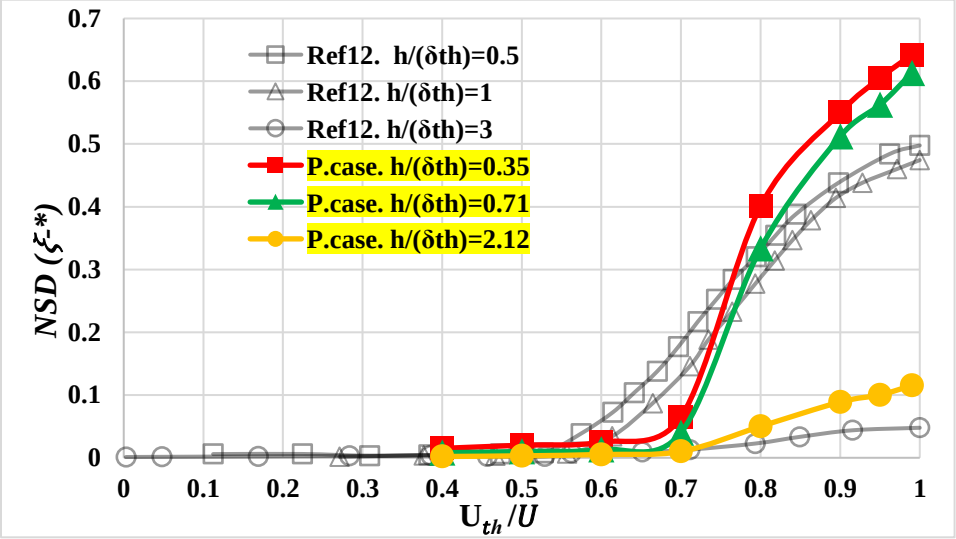

Figure 52: NSD vorticity for λ=200 µm compared to validated case A

As the U_{th}/U volume speed increases, the Re number decreases and the Strouhal number increases. The figure 53 shows the maximum number of Reynolds and St that can be reached when the mixing due to combined effect is reached. As with increase in λ also results in increment of δth and t_{rel} dominating the heat wave effect with maximum efficiency ≥0.69. So, Reynolds number further decreases for this case and St increases accordingly. From fig 53 Re number for ΔT 30K is 4.29×10^{-3} which is less than the already discussed cases. Further it reduces to 2.85×10^{-3} for ΔT 20K and 0.715×10^{-3} for ΔT 5K. With same reduction of Re the St number faces climb as 5.24×10^{-2} for ΔT 30K and this values also rises to 7.86×10^{-2} and $31.43\times10^{-2}$for ΔT 20K and 5K respectively.

Table 7: Variation of Re and St for λ=200 µm

ΔT	U_{th}U	U_{th}/U	ΔP	Re*1000	St /100	2*St /100
20K	0.97	0.97	0.4	0.206	54.43	108.87
	0.95	0.95	0.7	0.351	31.99	63.97
	0.9	0.9	1.4	0.741	15.15	30.3
	0.8	0.8	3.2	1.668	6.73	13.47
	0.7	0.7	5.4	2.859	3.93	7.86
	0.6	0.6	8.5	4.448	2.53	5.05
	0.5	0.5	12.7	6.672	1.68	3.37
	0.4	0.4	19	10.007	1.12	2.24
	0.3	0.3	29.6	15.567	0.72	1.44
	0.2	0.2	50.7	26.686	0.42	0.84
30K	0.97	0.97	0.6	0.31	36.29	72.58
	0.95	0.95	1	0.527	21.32	42.65
	0.9	0.9	2.1	1.112	10.1	20.2
	0.8	0.8	4.8	2.502	4.49	8.98
	0.7	0.7	8.2	4.289	2.62	5.24
	0.6	0.6	12.7	6.672	1.68	3.37
	0.5	0.5	19	10.007	1.12	2.24
	0.4	0.4	28.5	15.011	0.75	1.5
	0.3	0.3	44.4	23.351	0.48	0.96
	0.2	0.2	76.1	40.029	0.28	0.56
5K	0.97	0.97	0.1	0.052	217.73	435.47
	0.95	0.95	0.2	0.088	127.95	255.89
	0.9	0.9	0.4	0.185	60.61	121.21
	0.8	0.8	0.8	0.417	26.94	53.87
	0.7	0.7	1.4	0.715	15.71	31.43
	0.6	0.6	2.1	1.112	10.1	20.2
	0.5	0.5	3.2	1.668	6.73	13.47
	0.4	0.4	4.8	2.502	4.49	8.98
	0.3	0.3	7.4	3.892	2.89	5.77
	0.2	0.2	12.7	6.672	1.68	3.37

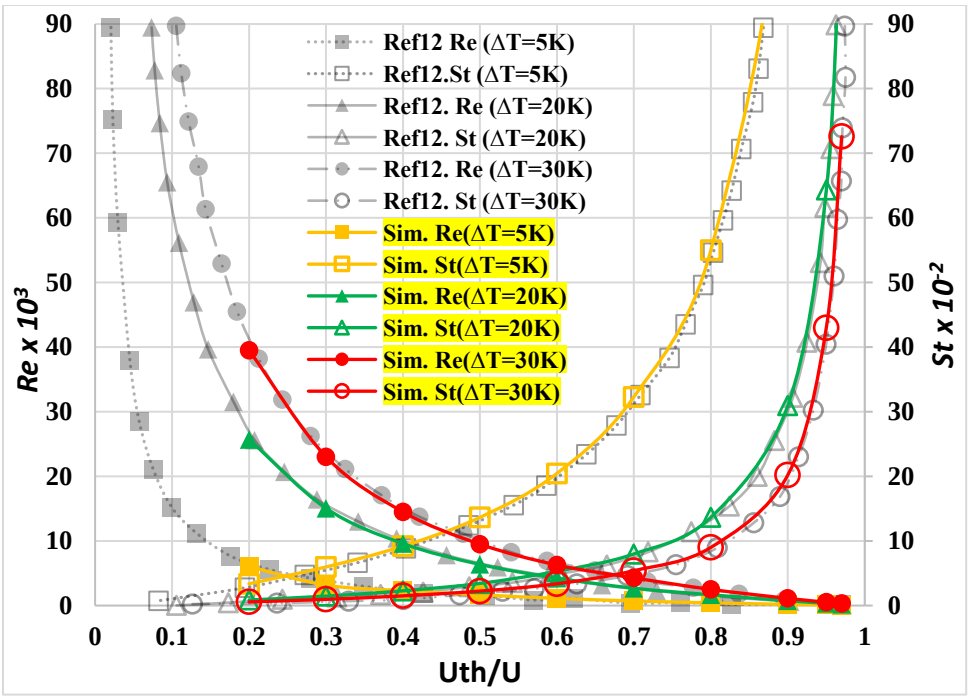

Figure 53: Variation of Re and St number for λ=200µm compared to the validated case A

For 200µm in Figures 54-57, normal total pressure, normal temperature, normal velocity u, and normal vortex lines for the 100th time step are shown in figures 54-57.

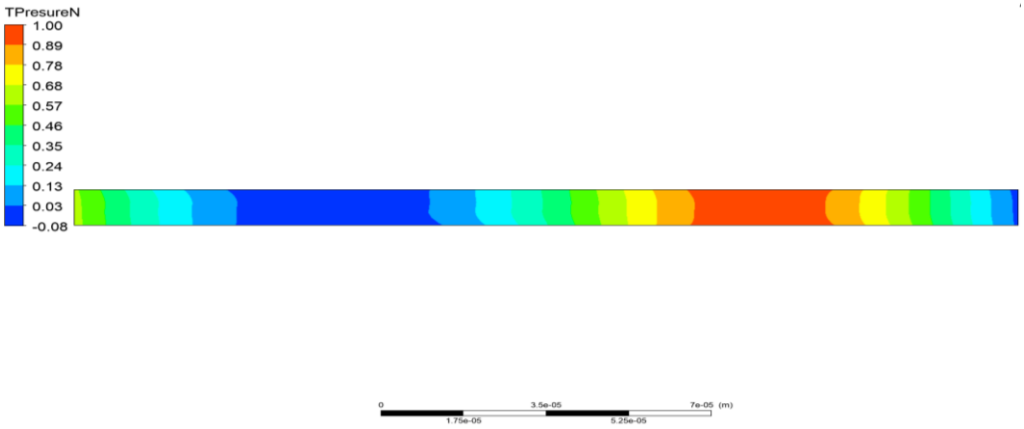

Figure 54: Normalized Pressure Variation for λ=200 µm

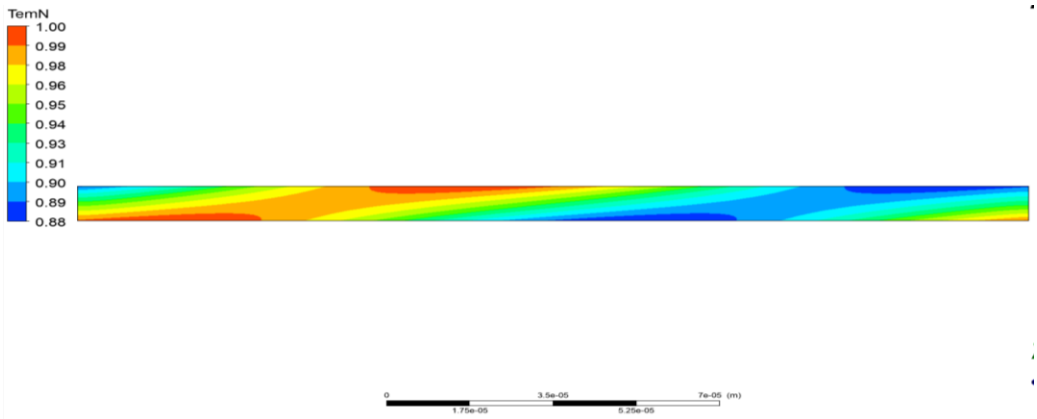

Figure 55: Normalized Temperature Variation for λ=200 µm

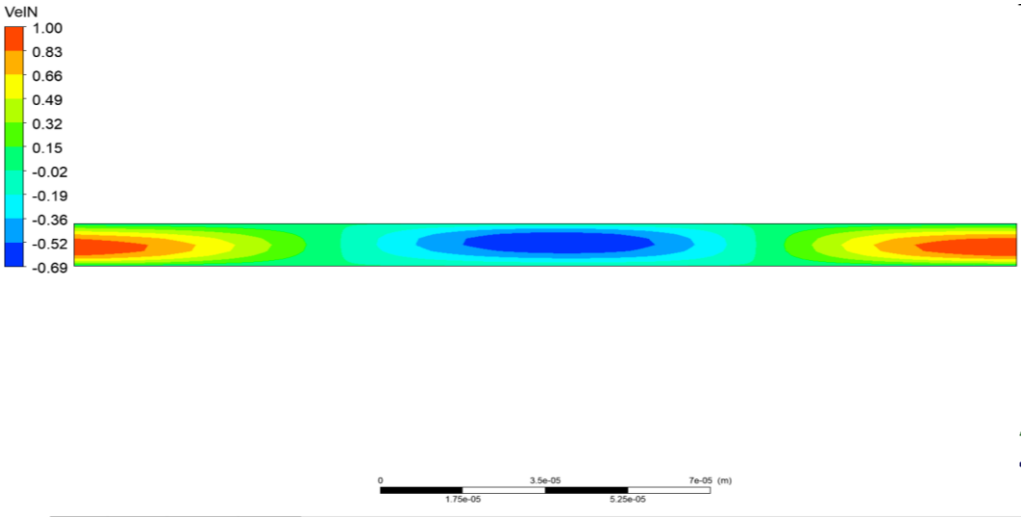

Figure 56: Normalized Velocity Variation for λ=200 µm

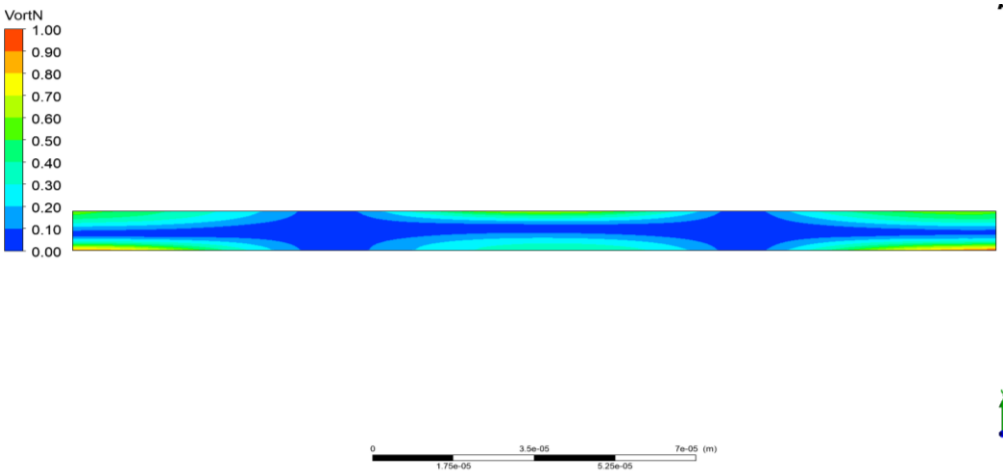

Figure 57: Normalized Vorticity Variation for λ=200 µm

5.4 CASE: D λ=50μm

Figures 58 to 64 show the variation of various parameters with the wavelength 50μm. Variation in mean vorticity is studied in figure 58. As the velocity is increased mean vorticity is decreased due to drop of differential pressure. It is clear from fig 58 that all graphs are separating from each other at approximately $U_{th}/U \geq 0.49$ showing that when λ decreases so heat wave diffusion length is restricted ($\delta_{th} \propto \sqrt{\lambda}$) to wall layers so differential pressure has a dominating role in mixing while TVEC effect is limited to layers close to the walls. Dimensionless mean vorticity can be enhanced by dropping the h/δ_{th} value from 4.25 to 0.7. It can be seen from the figure 58 that the maximum value of 1.25 exits for ReSt value of 1.8 and minimum at 1.15 for ReSt of 4.1, close to region where the Poiseuille flow is dominant. These values change to 0.8 and 0.55 for area dominant by thermal wave induced mixing at ReSt value of 1.8 and 4.1, respectively. Thermal penetration length decreased to 3.33 to 2.36 μm, 10 to 7.04 μm and 20 to 14.28 μm with corresponding increase of values of h/δ_{th} from 3 to 4.24 ,1 to 1.42 and 0.5 to 0.7, respectively. So, by comparing with validated case maximum value of chaotic mixing ($\bar{\xi}^*$ **)** due to TVEC effect is decreased from 0.77 which is lower to validated case A value (1.1).

Table 8: Variation of Vorticity and NSD vorticity for λ=50 μm

λ (μm)	h/δ_{th}	$U_{th}U$	U_{th}/U	ΔP	ReSt	Vorticity $\bar{\xi}^*$	NSD ($\bar{\xi}^*$)
50	0.702	0.400	0.143	60.895	1.80	1.191	0.021
50	0.702	0.500	0.200	40.597	1.80	1.120	0.028
50	0.702	0.600	0.273	27.064	1.80	1.034	0.035
50	0.702	0.700	0.368	17.399	1.80	0.931	0.049
50	0.702	0.800	0.500	10.149	1.80	0.817	0.101
50	0.702	0.900	0.692	4.511	1.80	0.724	0.211
50	0.702	0.950	0.826	2.137	1.80	0.722	0.280
50	0.702	0.990	0.961	0.410	1.80	0.777	0.401
50	1.416	0.400	0.143	91.533	2.70	1.152	0.009
50	1.416	0.500	0.200	61.022	2.70	1.081	0.013
50	1.416	0.600	0.273	40.681	2.70	0.994	0.021
50	1.416	0.700	0.368	26.152	2.70	0.888	0.033
50	1.416	0.800	0.500	15.255	2.70	0.763	0.075
50	1.416	0.900	0.692	6.780	2.70	0.642	0.170
50	1.416	0.950	0.826	3.212	2.70	0.616	0.240
50	1.416	0.990	0.961	0.616	2.70	0.649	0.370

50	4.25	0.40	0.14	138.92	4.10	1.09	0.002
50	4.25	0.50	0.20	92.61	4.10	1.02	0.003
50	4.25	0.60	0.27	61.74	4.10	0.94	0.011
50	4.25	0.70	0.37	39.69	4.10	0.83	0.015
50	4.25	0.80	0.50	23.15	4.10	0.70	0.035
50	4.25	0.90	0.69	10.29	4.10	0.57	0.042
50	4.25	0.95	0.83	4.87	4.10	0.53	0.048
50	4.25	0.99	0.96	0.94	4.10	0.54	0.063

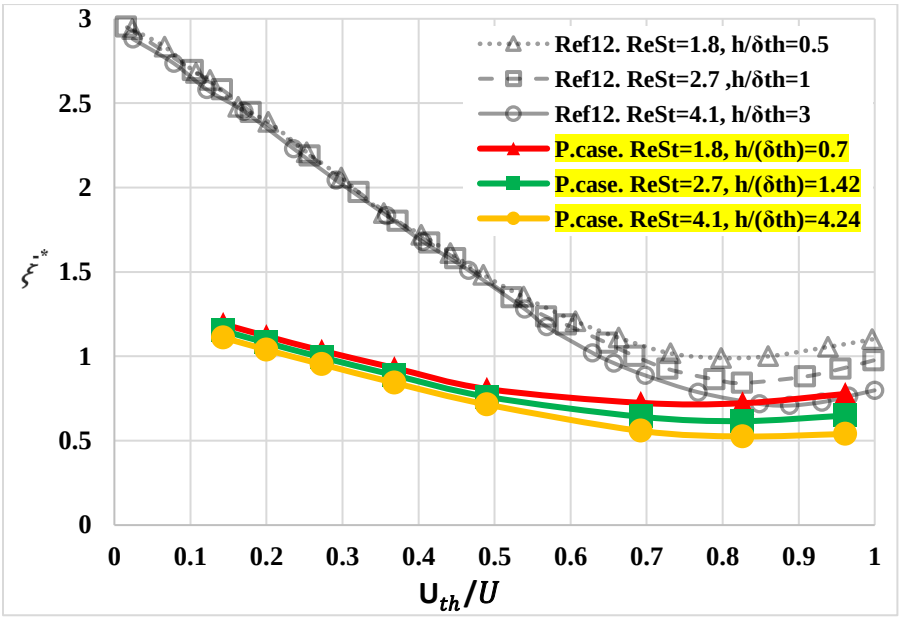

Figure 58: Dimensionless mean vorticity for λ= 50μm compared to validated case A

Normalized Standard Deviation (NSD) plots of vorticity are given in Figure 59. For λ=50μm values of h/δth varies from 0.7 to 4.24. These values enlarged as compared to validated case of 100μm wavelength as because δth is declining due to small wavelength resulting in enhancement of the non-dimensional number h/δ_{th}. NSD is growing up as the velocity ratio is moving up and all curves start to deviate from standard apparently at approximately $U_{th}/U \geq 0.49$. NSD can be enhanced by reducing the h/δ_{th} values. From fig 59 as the dimensionless velocity increases these values also increase reaching a top NSD vorticity of 0.401, 0.371 and 0.06 for h/ δ_{th} values of 0.7, 1.42 and 4.25, respectively. So, for larger values of Δp fluid flow steadily and experiences small

actuations in velocity field so when thermal effect is dominated due to small values of pressure fluid face higher whirling complex structures which contributes towards mixing enhancement.

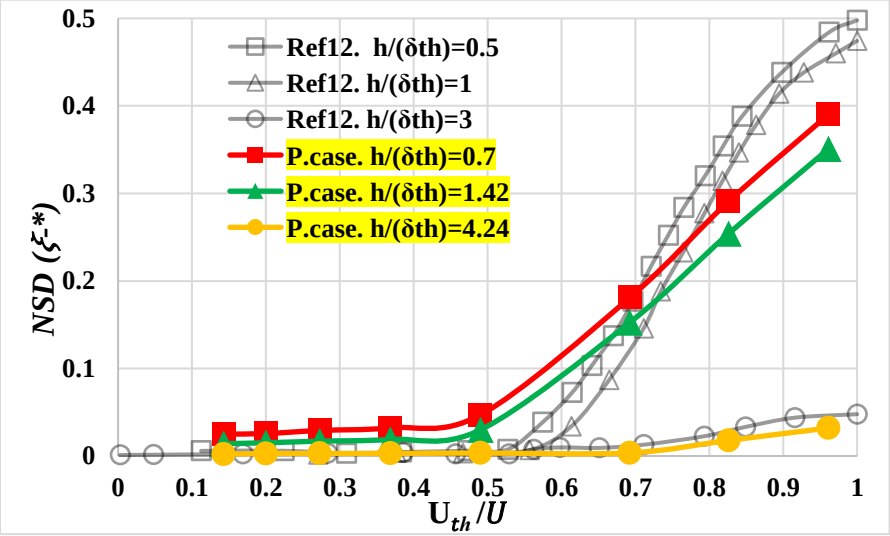

Figure 59: NSD vorticity for λ= 50µm compared to validated case A

It can be seen from figure 60 that as the dimensionless velocity U_{th}/U increases the Re number experiences a drop, while Strouhal number experience a climb, but these variations are somewhat different from previous cases due to that λ is decreasing so heat penetration distance in fluid is also falling (equation 8). Re number decreases but values are higher as compared to enhanced wavelength cases. In the same way St experiences an elevation but not in great order due to small diffusion length of heat in the fluid domain. The figure 60 demonstrates that the maximum bound of Reynold number that can be achieved for a ΔT of 30K is 11×10^{-3}.This value decreases to 7.72×10^{-3} and 1.9×10^{-3} for ΔT 20K and 5K, respectively. Correspondingly Strouhal number finds an augmentation meticulously as compared to last conferred cases due to low rate fall of Re number. The maximum value of Strouhal number that can be achieved with a ΔT of 5K is 12.1×10^{-2} which was 30×10^{-2} in previous case at ΔT of 5K. So, in this case this value drops to 3.1×10^{-2} and 2.17×10^{-2} for ΔT of 20K and 30K, respectively.

Table 9: Variation of Re and St for λ=50 μm

ΔT	$U_{th}U$	U_{th}/U	ΔP	Re*1000	St /100	2*St /100
20K	0.97	0.89	0.4	0.825	13.61	27.22
	0.95	0.826	0.7	1.405	8	15.99
	0.9	0.692	1.4	2.965	3.79	7.58
	0.8	0.5	3.2	6.672	1.68	3.37
	0.7	0.368	5.4	11.437	0.98	1.96
	0.6	0.273	8.5	17.791	0.63	1.26
	0.5	0.2	12.7	26.686	0.42	0.84
	0.4	0.143	19	40.029	0.28	0.56
	0.3	0.097	29.6	62.268	0.18	0.36
	0.2	0.059	50.7	106.745	0.11	0.21
30K	0.97	0.89	0.6	1.238	9.07	18.14
	0.95	0.826	1	2.107	5.33	10.66
	0.9	0.692	2.1	4.448	2.53	5.05
	0.8	0.5	4.8	10.007	1.12	2.24
	0.7	0.368	8.2	17.155	0.65	1.31
	0.6	0.273	12.7	26.686	0.42	0.84
	0.5	0.2	19	40.029	0.28	0.56
	0.4	0.143	28.5	60.044	0.19	0.37
	0.3	0.097	44.4	93.402	0.12	0.24
	0.2	0.059	76.1	160.118	0.07	0.14
5K	0.97	0.89	0.1	0.206	54.43	108.87
	0.95	0.826	0.2	0.351	31.99	63.97
	0.9	0.692	0.4	0.741	15.15	30.3
	0.8	0.5	0.8	1.668	6.73	13.47
	0.7	0.368	1.4	2.859	3.93	7.86
	0.6	0.273	2.1	4.448	2.53	5.05
	0.5	0.2	3.2	6.672	1.68	3.37
	0.4	0.143	4.8	10.007	1.12	2.24
	0.3	0.097	7.4	15.567	0.72	1.44
	0.2	0.059	12.7	26.686	0.42	0.84

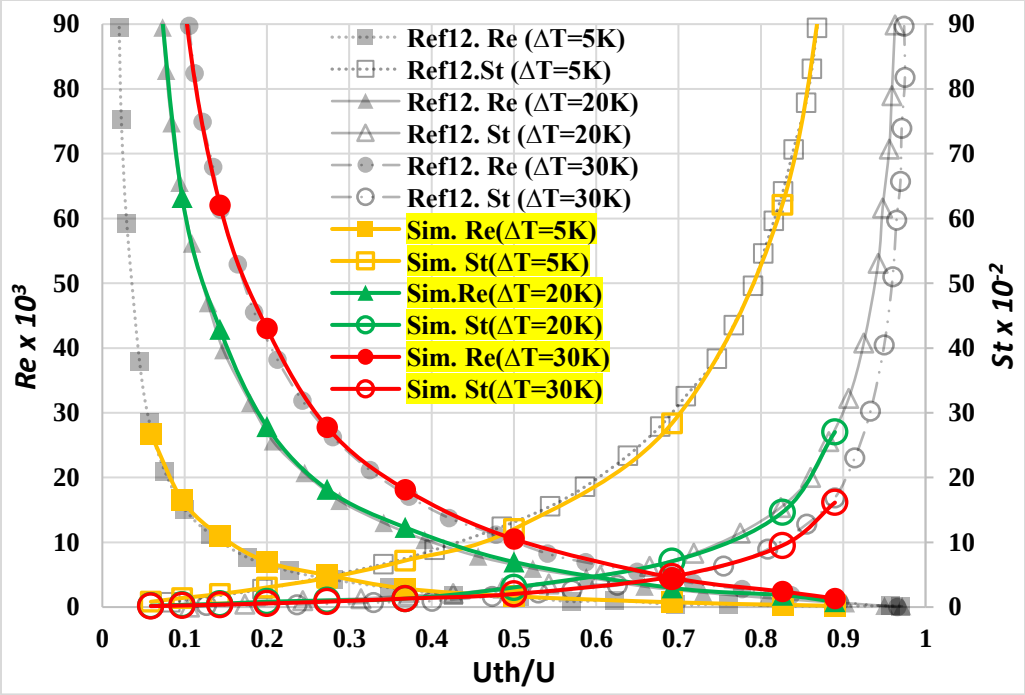

Figure 60: Variation of Re and St for λ=50µm compared to validated case A

Contours of Normalized total pressure, Normalized temperature, Normalized velocity u and Normalized vorticity at 100th time step is plotted for lambda 50 micrometer.

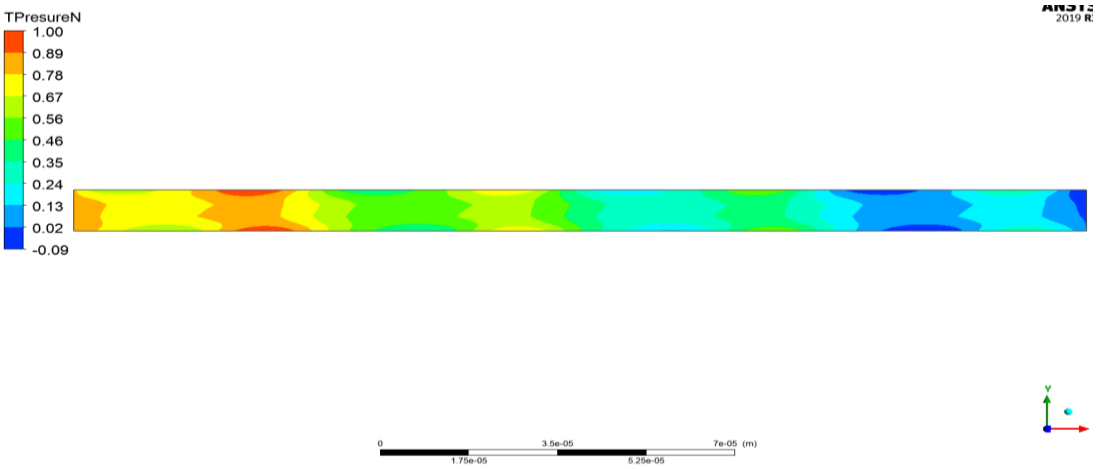

Figure 61: Normalized Pressure Variation for λ=50 µm

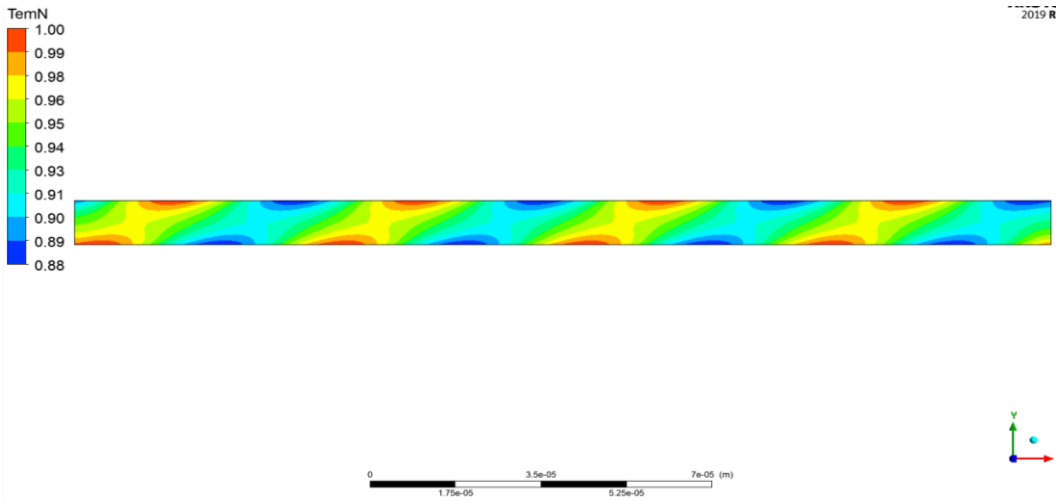

Figure 62: Normalized Temperature Variation for λ=50 µm

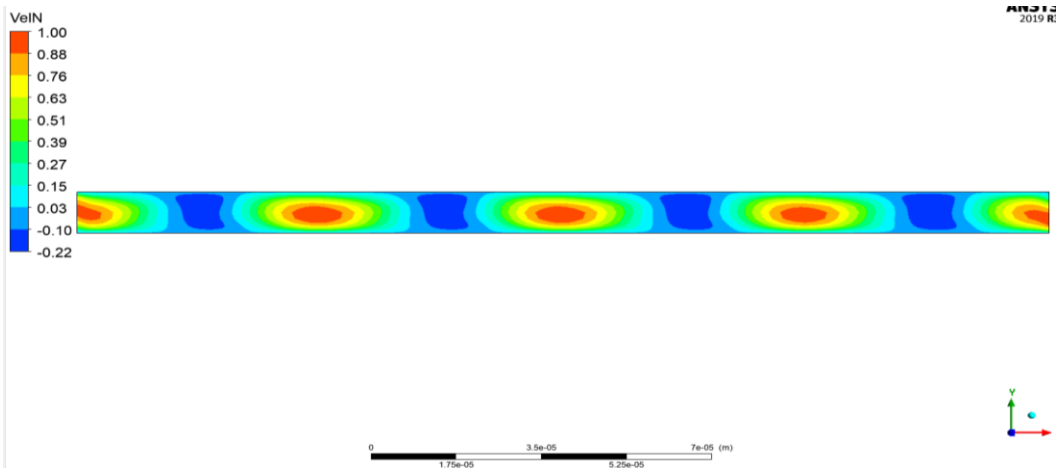

Figure 63: Normalized Velocity Variation for λ=50 µm

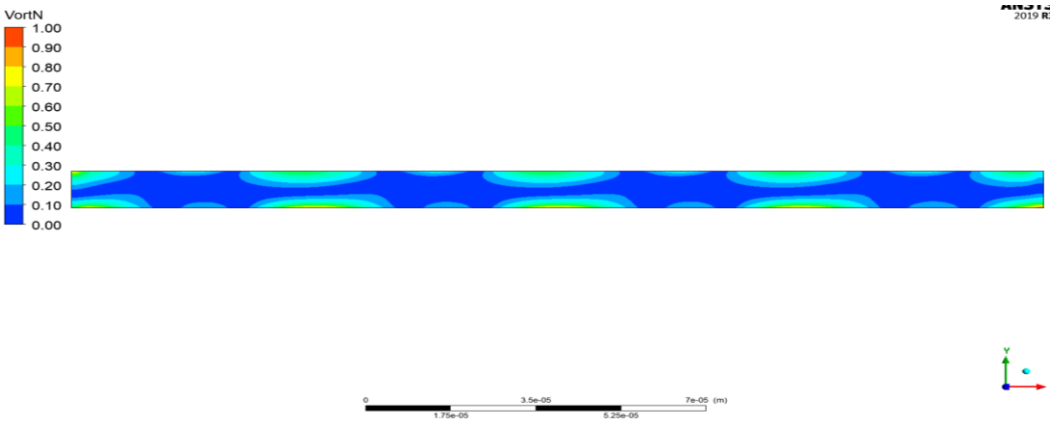

Figure 64: Normalized Vorticity Variation for λ=50 µm

5.5 Conclusion

The analysis was accomplished to understand the effects of wavelength on the micro channel parameters. In micro channel the chaotic mixing is directly related to the wavelength variation. The expansion and contraction effects are directly related to the chaotic mixing.

In this study, the effect of thermal viscous expansion and contraction is used to create flow turbulence at microchannels and formed appropriate circumstances for mixing liquids through transient simulations in the microchannel. The magnitude of chaos was studied by changing of wavelength. When differential pressure and opposite travelling thermal waves act on a microchannel, they produce chaotic mixing. The flow produced by the combined effect of TVEC and Δp results in homogenous mixing even at very low Reynolds number in order of 10^{-3} .

As the wavelength of these waves increase it was observed that thermal mixing length and relaxation time for mixing were increased. Moreover, it was also observed that as the wavelength increase the normalized mean vorticity also increases resulting in lowering of Reynolds number and incrementing of St number which is best for chaotic mixing at micro level study.

It is concluded that proper chaos flow and chaotic mixing are achieved at some specific value of non-dimensional number U_{th}/U, further mixing efficiency is strongly affected by another nondimensional number h/δ_{th}. So, for every specific value of λ corresponds to a certain minimum value of U_{th}/U upon which chaotic mixing is accomplished and further enhanced by lowering h/δ_{th} values.

When λ is increased from 100→150μm mixing efficiency due to TVEC effect increased from 0.54→0.64, max value of time average dimensionless mean vorticity ($\bar{\xi}^*$)increased from 1.1→1.23, max value of NSD ($\bar{\xi}^*$) increased from 0.49→0.55, min. value of Re 1.43→0.95 as a result St climbed up to max value 15.72→23.86.
When λ=100→200μm, mixing efficiency due to TVEC effect increased from 0.54→0.7, max value of $\bar{\xi}^*$ increased 1.1→1.4, NSD ($\bar{\xi}^*$) goes up 0.49→0.64, min. value of Re at which chaotic mixing is achieved drops to 1.43→0.72 as a result St climbed up to max value 15.72→32.29.
When λ=100→50μm mixing efficiency due to TVEC effect is reduced 0.54→0.49, max value of $\bar{\xi}^*$ falls as 1.1→0.77, NSD ($\bar{\xi}^*$) also face drop 0.49→0.39, min. value of Re 1.43→1.67which is

somewhat higher because U_{pois} is higher, conversely St max value 15.72→12.05 which increased little because small drop of Re number.

Finally, it was conferred that Reynold and Strouhal numbers have the great impact on proper disordered mixing which was obtained by growing St number which causes higher values of whirling motion of fluid in microchannel. Elevating St number is only possible when Re number decreases with same order because product of these two numbers (ReSt) is constant. So, declining Re number with Δp results in greater values St which is best for proper homogenous mixing.

REFERENCES

[1] Hessel, V.; Lowe, H.; Schonfeld, F. Micromixers—A review on passive and active mixing principles. Chem. Eng. Sci. 2005, 60, 2479-2501.

[2] Nguyen, N.-T.; Wu, Z. Micromixers—A review. J. Micromech. Microeng. 2005, 15, R1-R16.

[3] Jayaraj, S.; Kang, S.; Suh, Y.K. A review on the analysis and experiment of fluid flow and mixing in micro-channels. J. Mech. Sci. Technol. 2007, 21, 536-548.

[4] Falk, L.; Commenge, J.-M. Performance comparison of micromixers. Chem. Eng. Sci. 2010, 65, 405-411.

[5] Aubin, J.; Ferrando, M.; Jiricny, V. Current methods for characterising mixing and flow in microchannels. Chem. Eng. Sci. 2010, 65, 2065-2093.

[6] Aref, H. Stirring by chaotic advection. J. Fluid Mech. 1984, 143, 1-21.

[7] Ottino, J.M. The Kinematics of Mixing: Stretching, Chaos, and Transport; Cambride University Press: Cambride, UK, 1989; pp. 180-182.

[8] Floyd, T.M.; Schmidt, M.A.; Jensen, K.F. Silicon micromixers with infrared detection for studies of liquid-phase reactions. Ind. Eng. Chem. Res. 2005, 44, 2351-2358.

[9] Nguyen, N.-T.; Huang, X. Mixing in microchannels based on hydrodynamic focusing and time-interleaved segmentation and experiment. Lab Chip 2005, 5, 1320-1326.

[10] Adeosun, J.T.; Lawal, A. Mass transfer enhancement in microchannel reactors by reorientation of fluid interfaces and stretching. Sens. Actuator. B 2005, 110, 101-111.

[11] Adeosun, J.T.; Lawal, A. Residence-time distribution as a measure of mixing in T-junction and multilaminated/elongational flow micromixers. Chem. Eng. Sci. 2010, 65, 1865-1874.

[12] A.H. Meghdadi Isfahani, Ramin Nasehi, Ebrahim Shirani, “Mixing enhancement in micro channels using thermos-viscous expansion by oscillating temperature wave”, Chemical engineering & processing 126 (2018) 123-131.

[13] Cha, J.; Kim, J.; Ryu, S.-K.; Park, J.; Jeong, Y.; Park, S.; Park, S.; Kim, H.C.; Chun, K. A highly efficient 3D micromixer using soft PDMS bonding. J. Micromech. Microeng.

2006, 16, 1778-1782.

[14] Park, H.Y.; Qiu, X.; Rhoades, E.; Korlach, J.; Kwok, L.W.; Zipfel, W.R.; Webb, W.W.; Pollack, L. Achieving uniform mixing in a microfluidic device: Hydrodynamic focusing prior to mixing. Anal. Chem. 2006, 78, 4465-4473.

[15] Cieslicki, K.; Piechna, A. Investigations of mixing process in microfluidic manifold designed according to biomimetic rule. Lab Chip 2009, 9, 726-732.

[16] MacInnes, J.M.; Chen, Z.; Allen, R.W.K. Investigation of alternating-flow mixing in microchannels. Chem. Eng. Sci. 2005, 60, 3453-3467.

[17] Goullet, A.; Glasgow, I.; Aubry, N. Effects of microchannel geometry on pulsed flow mixing, Mech. Res. Commun. 2006, 33, 739-746.

[18] Coleman, J.T.; Sinton, D. A sequential injection microfluidic mixing strategy. Microfluid Nanofluid 2005, 1, 319-327.

[19] Coleman, J.T.; McKechnie, J.; Sinton, D. High-efficiency electrokinetic micromixing through symmetric sequential injection and expansion. Lab Chip 2006, 6, 1033-1039.

[20] Leong, J.-C.; Tsai, C.-H.; Chang, C.-L.; Lin, C.-F.; Fu, L.-M. Rapid microfluidic mixers utilizing dispersion effect and interactively time-pulsed injection. Jpn. J. Appl. Phys. 2007, 46, 5345-5352.

[21] Sun, C.-L.; Sie, J.-Y. Active mixing in diverging microchannel. Microfluid Nanofluid 2010, 8, 485-495.

[22] Fu, L.-M.; Tsai, C.-H. Design of interactively time0pulsed microfluidic mixers in microchips using numerical simulation. Jpn. J. Appl. Phys. 2007, 46, 420-429.

[23] Lee, Y.-K.; Shih, C.; Tabeling, P.; Ho, C.-M. Experimental study and nonlinear dynamic analysis of time-periodic micro chaotic mixers. J. Fluid Mech. 2007, 575, 425-448.

[24] Chen, C.-K.; Cho, C.-C. A combined active/passive scheme for enhancing the mixing efficiency of microfluidic devices. Chem. Eng. Sci. 2008, 63, 3081-3087.

[25] Liu, R.H.; Stremler, M.A.; Sharp, K.V.; Olsen, M.G.; Santiego, J.G.; Adrian, R.J.; Aref, H.; Beebe, D.J. Passive mixing in a three-dimensional serpentine microchannel. J. Microelectromech. Syst. 2000, 9, 190-197.

[26] Stroock, A.D.; Dertinger, S.W.; Ajdari, A.; Mezic, I.; Stone, A.; Whitesides, G.M. Chaotic mixer for microchannels. Science 2002, 295, 647-651.

[27] Heo, H.S.; Suh, Y.K. Enhancement of stirring in a straight channel at low Reynolds-numbers with various block-arrangement. J. Mech. Sci. Technol. 2005, 19, 199-208.

[28] Kim, D.S.; Lee, S.H.; Kwon, T.H.; Ahn, C.H. A serpentine laminating micromixer combining splitting/recombination and advection. Lab Chip 2005, 5, 739-747.

[29] Xia, H.M.; Wan, S.Y.M.; Shu, C.; Chew, Y.T. Chaotic micromixers using two-layer crossing channels to exhibit fast mixing at low Reynolds numbers. Lab Chip 2005, 5, 748-755.

[30] Ansari, M.A.; Kim, K.-Y. Parametric study on mixing of two fluids in a three-dimensional serpentine microchannel. Chem. Eng. Sci. 2009, 146, 439-448.

[31] Howell, P.B.; Mott, D.R.; Fertig, S.; Kaplan, C.R.; Golden, J.P.; Oran, E.S.; Ligler, F.S. A microfluidic mixer with grooves placed on the top and bottom of the channel. Lab Chip 2005, 5, 524-530.

[32] Yang, J.-T.; Huang, K.-J.; Tung, K.-Y.; Hu, I.-C.; Lyu, P.-C. A chaotic micromixer modulated by constructive vortex agitation. J. Micromech. Microeng. 2007, 17, 2084-2092.

[33] Simonnet, C.; Groisman, A. Chaotic mixing in a steady flow in a microchannel. Phys. Rev. Lett. 2005, 94, 134501.

[34] Camesasca, M.; Kaufman, M.; Manas-Zloczower, I. Staggered passive micromixers with fractal surface patterning. J. Micromech. Microeng. 2006, 16, 2298-2311.

[35] Yang, J.-T.; Fang, W.-F.; Tung, K.-Y. Fluids mixing in devices with connected-groove channels. Chem. Eng. Sci. 2008, 63, 1871-1881.

[36] Hardt, S.; Pennemann, H.; Schonfeld, F. Theoretical and experimental characterization of a low- Reynolds number split-and-recombine mixer. Microfluid Nanofluid 2006, 2, 237-248.

[37] Lee, S.W.; Kim, D.S.; Lee, S.S.; Kwon, T.H. A split and recombination micromixer fabricated in a PDMS three-dimensional structure. J. Micromech. Microeng. 2006, 16, 1067-1072.

[38] Suh, Y.K.; Heo, S.G.; Heo, Y.G.; Heo, H.S.; Kang, S. Numerical and experimental study on a channel mixer with a periodic array of cross baffles. J. Mech. Sci. Technol. 2007, 21, 549-555.

[39] Zhang, J.-B.; He, G.-W.; Liu, F. Electro-osmotic flow and mixing in heterogeneous microchannels. Phys. Rev. E 2006, 73, 056305.

[40] Chen C.-K.; Cho C.-C. Electrokinetically-driven flow mixing in microchannels with avy surface. J. Colloid Interface Sci. 2007, 312, 470-480.

[41] Wu, Z.; Li, D. Micromixing using induced-charge electrokinetic flow. Electrochim. Acta 2008, 53, 5827-5835.

[42] Kang, J.; Heo, H.S.; Suh, Y.K. LBM simulation on mixing enhancement by the effect of heterogeneous zeta-potential in a microchannel. J. Mech. Sci. Technol. 2008, 22, 1181-1191.

[43] Qian, S.; Bau, H.H. Theoretical investigation of electro-osmotic flows and chaotic stirring in rectangular cavities. Appl. Math. Modell. 2005, 29, 726-753.

[44] Zhao, H.; Bau, H.H. Microfluidic chaotic stirrer utilizing induced-charge electro-osmosis. Phys. Rev. E 2007, 75, 066217.

[45] Wu, H.-Y.; Liu, C.-S. A novel electrokinetic micromixer. Sens. Actuator. A 2005, 118, 107-115.

[46] Sasaki, N.; Kitamori, T.; Kim, H.-B. Ac electroosmotic micromixer for chemical processing in a microchannel. Lab Chip 2006, 6, 550-554.

[47] Huang, S.-H.; Wang, S.-K.; Khoo, H.S.; Tseng, F.-G. Ac electroosmotic generated in-plane microvortices for stationary or continuous fluid mixing. Sens. Actuator. B 2007, 125, 326-336.

[48] Shin, S.M.; Kang, I.S.; Cho,Y.-K. Mixing enhancement by using electrokinetic instability under time-periodic electric field. J. Micromech. Microeng. 2005, 15, 455-462.

[49] Chun, H.; Kim, H.C.; Chung, T.D. Ultrafast active mixer using polyelectrolytic ion extractor. Lab Chip 2008, 8, 764-771.

[50] Liau, A.; Kamik, R.; Majumdar, A.; Cate, J.H.D. Mixing crowded biological solutions in milliseconds. Anal. Chem. 2005, 77, 7618-7625.

[51] Muradoglu, M.; Stone, H. Mixing in a drop moving through a serpentine channel: A computational study. Phys. Fluids 2005, 17, 073305.

[52] Tung, K.-Y.; Li, C.-C.; Yang, J.-T. Mixing and hydrodynamic analysis of a droplet in a planar serpentine micromixer. Microfluid Nanofluid 2009, 7, 545-557.

[53] Dogan, H.; Nas, S.; Muradoglu, M. Mixing of miscible liquids in gas-segmented serpentine channels, Int. J. Multiphase Flow 2009, 35, 1149-1158.

[54] Tanthapanichakoon, W.; Aoki, N.; Matsuyama, K.; Mae, K. Design of mixing in microfluidic liquid slugs based on a new dimensionless number for precise reaction and mixing operation. Chem. Eng. Sci. 2006, 61, 4220-4232.

[55] Wang, Y.; Kang, S.; Suh, Y.K. Enhancement of mixing in a microchannel by using ac-electroosmotic effect. In Proceedings of Micro/Nanoscale Heat Transfer Conf., Taiwan 2008; Paper No. MNHT2008-52142.

[56] Sarrazin, F.; Prat, L.; Miceli, N.D.; Cristobal, G.; Link, D.R.; Weitz, D.A. Mixing characterization inside microdroplets engineered on a microcoalescer. Chem. Eng. Sci. 2007, 62, 1042-1048.

[57] Rhee, M.; Burns, M.A. Drop mixing in a microchannel for lab-on-a-chip platform. Langmuir, 2008, 24, 590-601.

[58] Grumann, M.; Riegger, A.G.L.; Zengerle, R.; Ducree, J. Batch-mode mixing on centrifugal microfluidic platforms. Lab Chip 2005, 5, 560-565.

[59] Kang, T.G.; Hulsen, M.A.; den Toonder, J.M.J.; Anderson, P.D.; Meijer, H.E.H. A direct simulation method of flows with suspended paramagnetic particles. J. Comput. Phys. 2008, 227, 4441-4458.

[60] Suh, Y.K.; Kang, S. Motion of paramagnetic particles submerged in a viscous fluid under a uniform magnetic field—Benchmark solutions. J. Eng. Math. 2010, doi: 10.1007/s10665-010-9364-1.

[61] Kang, S.; Suh, Y.K. An immersed-boundary finite-volume method for direct simulation of flows with suspended paramagnetic particles. Int. J. Numer. Methods Fluids 2010, doi: 10.1002/fld.2336.

[62] Calhoun, R.; Yadav, A.; Phelan, P.; Vuppu, A.; Garcia, A.; Hayes, M. Paramagnetic particles and mixing in micro-scale flows. Lab Chip 2006, 6, 247-257.

[63] Franke, T.; Schmid, L.; Weitz, D.A.; Wixforth, A. Magneto-mechanical mixing and manipulation of picoliter volumes in vesciles. Lab Chip 2009, 9, 2831-2835.

[64] Lee, S.H.; von Noort, D.; Lee, J.Y.; Zhang, B.-T.; Park, T. H. Effective mixing in a microfluidic chip using magnetic particles. Lab Chip 2009, 9, 479-482.

[65] Roy, T.; Sinha, A.; Chakraborty, S.; Ganguly, R.; Puri, I.K. Magnetic microsphere-based mixers for microdroplets. Phys. Fluids 2009, 21, 027101.

[66] Le, T.N.; Suh, Y.K.; Kang, S. A numerical study on the flow and mixing in a microchannel using magnetic particles. J. Mech. Sci. Technol. 2010, 24, 441-450.

[67] Kim, M.J.; Breuer, K.S. Controlled mixing in microfluidic systems using bacterial chemotaxis, Anal. Chem. 2007, 79, 955-959.

[68] Hardt, S.; Drese, K.S.; Hessel, V.; Schönfeld, F. "Passive micromixers for applications in the micro reactor and μTAS fields", Microfluid *Nanofluid* **2005**, *1*, 108-118.

APPENDIX A

Nomenclature

A	Area element
c_p	Specific heat capacity at constant pressure
h	Micro channel height
k	Conductivity
L	Micro channel length
NSD	Normalized Standard Deviation
p	Pressure
P_r	Prandtl number
Re	Reynolds number
St	Strouhal number
t	time Temperature
U	Characteristic velocity in x_1 direction
V	Characteristic velocity in x_2 direction

Greek symbols

α_T	Volumetric thermal expansion coefficient
α	Thermal diffusivity
δ_{kl}	Kronecker delta
$\delta_{th.}$	Thermal penetration length
ε	Small number
η_T	Thermal viscosity coefficient
θ	Dimensionless Temperature
λ	Thermal wavelength
μ	Viscosity
ϑ	Kinematic viscosity
ξ	Vorticity
ρ	Density
Φ	Rate of viscous dissipation
χ	Free function
ω	Thermal wave frequency
∞	Infinite number
∂	Partial derivative symbol
∇	Partial derivative operator

Subscripts

1,2	Horizontal and lateral directions
0	Reference state
▪	Dimensionless parameters Mean
$\sim$	Time average
$th.$	Vector Thermal
$h.$	Hydrodynamic
Poi	Poiseuille flow

APPENDIX B

CFX Command Language for Run

```
LIBRARY:
 CEL:
  EXPRESSIONS:
   BettaT = 2.97e-04[K^-1]
   Dens = Ro0*(1.0-BettaT*(T- T0))
   DownWallTemp = T0+T1*sin((2*pi*x+ut*t)/landa)
   EttaT = 0.0215[K^-1]
   InitialTemp = T0+T1*sin(2*pi*x/landa)
   L = 200e-6 [m]
   Pr = nu0/alpha0
   Pref = 1[atm]
   Re = Upois*h/nu0
   ReSt = Re*st
   Ro0 = 999.5 [kg m^-3]
   T0 = (273.15+30 )[K]
   T1 = 20.0[K]
   UpWallTemp = T0+T1*sin((2*pi*x-ut*t)/landa)
   Upois = h ^2*deltaP /(12*mu0*landa)
   Uth = BettaT *T1*ut
   UthToU = Uth/Utotal
   UthU = 0.9
   Utotal = Uth+Upois
   alpha0 = 4.8e-07 [m^2/s]
   deltaP = deltaP000*(L/landa)
   deltaP000 = ((12*mu0 *T1*landa*BettaT*ut)/(h^2))*((1/UthU)-1)
   deltath = sqrt(alpha0*landa/ut)
   h = 10e-06 [m]
   hTodeltath = h/deltath
   landa = 100.0e-06[m]
   mu = mu0*(1.0-EttaT*(T- T0))
   mu0 = 0.0008899[Pa s]
   nu = mu/Dens
   nu0 = mu0/Ro0
   omega = ut/landa
   st = omega*tRel
   tRel = landa/Upois
   timePeriod = (landa*pi*2)/ut
   tscale = landa/ut
   tstep = 0.01*(tscale)
   ut = 0.481[m/s]
  END
 END
 MATERIAL: Material 1
  Coord Frame = Coord 0
  Material Group = Water Data
  Option = Pure Substance
  Thermodynamic State = Liquid
  PROPERTIES:
   Option = General Material
   EQUATION OF STATE:
    Density = Dens
```

```
    Molar Mass = 1.0 [kg kmol^-1]
    Option = Value
   END
   REFERENCE STATE:
    Option = Specified Point
    Reference Pressure = 1 [atm]
    Reference Temperature = 300 [K]
   END
   DYNAMIC VISCOSITY:
    Dynamic Viscosity = mu
    Option = Value
   END
  END
 END
 MATERIAL: Water
  Material Description = Water (liquid)
  Material Group = Water Data,Constant Property Liquids
  Option = Pure Substance
  Thermodynamic State = Liquid
  PROPERTIES:
   Option = General Material
   EQUATION OF STATE:
    Density = Dens
    Molar Mass = 18.02 [kg kmol^-1]
    Option = Value
   END
   SPECIFIC HEAT CAPACITY:
    Option = Value
    Specific Heat Capacity = 4181.7 [J kg^-1 K^-1]
    Specific Heat Type = Constant Pressure
   END
   REFERENCE STATE:
    Option = Specified Point
    Reference Pressure = Pref
    Reference Specific Enthalpy = 0.0 [J/kg]
    Reference Specific Entropy = 0.0 [J/kg/K]
    Reference Temperature = T0
   END
   DYNAMIC VISCOSITY:
    Dynamic Viscosity = mu
    Option = Value
   END
   THERMAL CONDUCTIVITY:
    Option = Value
    Thermal Conductivity = 0.6069 [W m^-1 K^-1]
   END
   ABSORPTION COEFFICIENT:
    Absorption Coefficient = 1.0 [m^-1]
    Option = Value
   END
   SCATTERING COEFFICIENT:
    Option = Value
    Scattering Coefficient = 0.0 [m^-1]
   END
   REFRACTIVE INDEX:
    Option = Value
```

```
      Refractive Index = 1.0 [m m^-1]
    END
    THERMAL EXPANSIVITY:
      Option = Value
      Thermal Expansivity = 2.57E-04 [K^-1]
    END
  END
 END
END
FLOW: Flow Analysis 1
 SOLUTION UNITS:
  Length Units = [m]
  Mass Units = [kg]
  Temperature Units = [K]
  Time Units = [s]
 END
 ANALYSIS TYPE:
  Option = Transient
  EXTERNAL SOLVER COUPLING:
   Option = None
  END
  INITIAL TIME:
   Option = Automatic with Value
   Time = 0 [s]
  END
  TIME DURATION:
   Option = Total Time
   Total Time = tscale
  END
  TIME STEPS:
   Option = Timesteps
   Timesteps = tstep
  END
 END
 DOMAIN: Default Domain
  Coord Frame = Coord 0
  Domain Type = Fluid
  Location = B16
  BOUNDARY: Symmetry
   Boundary Type = SYMMETRY
   Location = F18.16
  END
  BOUNDARY: Symmetry1
   Boundary Type = SYMMETRY
   Location = rightwall
  END
  BOUNDARY: bottomwall
   Boundary Type = WALL
   Location = F21.16
   BOUNDARY CONDITIONS:
    HEAT TRANSFER:
     Fixed Temperature = DownWallTemp
     Option = Fixed Temperature
    END
    MASS AND MOMENTUM:
     Option = No Slip Wall
```

```
    END
  END
END
BOUNDARY: inlet
  Boundary Type = OPENING
  Location = inlet
  BOUNDARY CONDITIONS:
    FLOW DIRECTION:
      Option = Normal to Boundary Condition
    END
    FLOW REGIME:
      Option = Subsonic
    END
    HEAT TRANSFER:
      Option = Static Temperature
      Static Temperature = 300 [K]
    END
    MASS AND MOMENTUM:
      Option = Opening Pressure and Direction
      Relative Pressure = deltaP
    END
  END
END
BOUNDARY: outlet
  Boundary Type = OPENING
  Location = F20.16
  BOUNDARY CONDITIONS:
    FLOW DIRECTION:
      Option = Normal to Boundary Condition
    END
    FLOW REGIME:
      Option = Subsonic
    END
    HEAT TRANSFER:
      Opening Temperature = 300 [K]
      Option = Opening Temperature
    END
    MASS AND MOMENTUM:
      Option = Opening Pressure and Direction
      Relative Pressure = 0 [Pa]
    END
  END
END
BOUNDARY: topwall
  Boundary Type = WALL
  Location = F19.16
  BOUNDARY CONDITIONS:
    HEAT TRANSFER:
      Fixed Temperature = UpWallTemp
      Option = Fixed Temperature
    END
    MASS AND MOMENTUM:
      Option = No Slip Wall
    END
  END
END
```

```
DOMAIN MODELS:
  BUOYANCY MODEL:
    Option = Non Buoyant
  END
  DOMAIN MOTION:
    Option = Stationary
  END
  MESH DEFORMATION:
    Option = None
  END
  REFERENCE PRESSURE:
    Reference Pressure = Pref
  END
END
FLUID DEFINITION: Fluid 1
  Material = Water
  Option = Material Library
  MORPHOLOGY:
    Option = Continuous Fluid
  END
END
FLUID MODELS:
  COMBUSTION MODEL:
    Option = None
  END
  HEAT TRANSFER MODEL:
    Include Pressure Transient Term = On
    Include Viscous Dissipation Term = On
    Option = Thermal Energy
  END
  THERMAL RADIATION MODEL:
    Option = None
  END
  TURBULENCE MODEL:
    Option = Laminar
  END
END
INITIALISATION:
  Coord Frame = Coord 0
  Option = Automatic
  INITIAL CONDITIONS:
    Velocity Type = Cartesian
    CARTESIAN VELOCITY COMPONENTS:
      Option = Automatic with Value
      U = 0 [m s^-1]
      V = 0 [m s^-1]
      W = 0 [m s^-1]
    END
    STATIC PRESSURE:
      Option = Automatic with Value
      Relative Pressure = 0 [Pa]
    END
    TEMPERATURE:
      Option = Automatic with Value
      Temperature = T0
    END
```

```
    END
  END
END
OUTPUT CONTROL:
  MONITOR OBJECTS:
    Monitor Coefficient Loop Convergence = On
    MONITOR BALANCES:
      Option = Full
    END
    MONITOR FORCES:
      Option = Full
    END
    MONITOR PARTICLES:
      Option = Full
    END
    MONITOR RESIDUALS:
      Option = Full
    END
    MONITOR TOTALS:
      Option = Full
    END
  END
  RESULTS:
    Extra Output Variables List = Vorticity
    File Compression Level = Default
    Option = Standard
  END
  TRANSIENT RESULTS: Transient Results 1
    File Compression Level = Default
    Option = Standard
    OUTPUT FREQUENCY:
      Option = Every Timestep
    END
  END
  TRANSIENT RESULTS: Transient Results 2
    Extra Output Variables List = Vorticity
    File Compression Level = Default
    Option = Standard
    OUTPUT FREQUENCY:
      Option = Every Timestep
    END
  END
  TRANSIENT STATISTICS: Transient Statistics 1
    Option = Arithmetic Average
    Output Variables List = Vorticity
  END
  TRANSIENT STATISTICS: Transient Statistics 2
    Option = Standard Deviation
    Output Variables List = Vorticity
  END
  TRANSIENT STATISTICS: Transient Statistics 3
    Option = Full
    Output Variables List = Vorticity
  END
  TRANSIENT STATISTICS: Transient Statistics 4
    Option = Root Mean Square
```

```
    Output Variables List = Vorticity
   END
  END
  SOLVER CONTROL:
   ADVECTION SCHEME:
    Option = High Resolution
   END
   CONVERGENCE CONTROL:
    Maximum Number of Coefficient Loops = 10
    Minimum Number of Coefficient Loops = 1
    Timescale Control = Coefficient Loops
   END
   CONVERGENCE CRITERIA:
    Residual Target = 0.00001
    Residual Type = RMS
   END
   INTERRUPT CONTROL:
    Option = Any Interrupt
    CONVERGENCE CONDITIONS:
     Option = Default Conditions
    END
   END
   TRANSIENT SCHEME:
    Option = Second Order Backward Euler
    TIMESTEP INITIALISATION:
     Option = Automatic
    END
   END
  END
 END
 COMMAND FILE:
END
 SIMULATION CONTROL:
  EXECUTION CONTROL:
      END
   PARALLEL HOST LIBRARY:
    HOST DEFINITION: hamidpc
     Remote Host Name = HAMID-PC
     Installation Root = f:\Program Files\ANSYS Inc\v%v\CFX
     Host Architecture String = winnt-amd64
    END
   END
   RUN DEFINITION:
    Solver Input File = \
     D:\100_projects\7_Microchannel-CFX+\fig6-2\fig62--1.def
    Run Mode = Full
    Solver Results File = \
     D:\100_projects\7_Microchannel-CFX+\fig6-2\fig62--1_001.res
   END
   SOLVER STEP CONTROL:
    PARALLEL ENVIRONMENT:
     Start Method = Serial
    END
   END
  END
 END
```